

<https://helda.helsinki.fi>

Self-Catalytic Reaction of SO₃ and NH₃ To Produce Sulfamic Acid and Its Implication to Atmospheric Particle Formation

Li, Hao

2018-09-05

Li , H , Zhong , J , Vehkamäki , H , Kurtén , T , Wang , W , Ge , M , Zhang , S , Li , Z , Zhang , X , Francisco , J S & Zeng , X C 2018 , ' Self-Catalytic Reaction of SO₃ and NH₃ To Produce Sulfamic Acid and Its Implication to Atmospheric Particle Formation ' , Journal of the American Chemical Society , vol. 140 , no. 35 , pp. 11020-11028 . <https://doi.org/10.1021/jacs.8b04928>

<http://hdl.handle.net/10138/271657>

<https://doi.org/10.1021/jacs.8b04928>

unspecified

acceptedVersion

Downloaded from Helda, University of Helsinki institutional repository.

This is an electronic reprint of the original article.

This reprint may differ from the original in pagination and typographic detail.

Please cite the original version.

Self-Catalytic Reaction of SO₃ and NH₃ to Produce Sulfamic Acid and Its Implication to Atmospheric New Particle Formation

Hao Li,^{1,2#} Jie Zhong,^{2#} Hanna Vehkamäki,³ Theo Kurtén,⁴ Weigang Wang,⁵ Maofa Ge,⁵ Shaowen Zhang,¹ Zesheng Li,¹ Xiuhui Zhang,^{1*} Joseph S. Francisco,^{2*} Xiao Cheng Zeng^{2,6*}

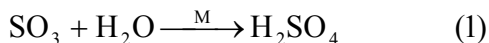
¹Key Laboratory of Cluster Science, Ministry of Education of China, School of Chemistry and Chemical Engineering, Beijing Institute of Technology, Beijing 100081, P. R. China; ²Department of Chemistry, University of Nebraska-Lincoln, Lincoln, NE, 68588, USA; ³Institute for Atmospheric and Earth System Research/Chemistry, University of Helsinki, PO Box 64 (Gustaf Hällströmin katu 2a), FI-00014, Helsinki, Finland; ⁴Institute for Atmospheric and Earth System Research/Chemistry, University of Helsinki, PO Box 64 (Gustaf Hällströmin katu 2a), FI-00014, Helsinki, Finland; ⁵Beijing National Laboratory for Molecular Sciences (BNLMS), State Key Laboratory for Structural Chemistry of Unstable and Stable Species, Institute of Chemistry, Chinese Academy of Sciences, 100190, Beijing, China; ⁶Beijing Advanced Innovation Center for Soft Matter Science and Engineering, Beijing University of Chemical Technology, Beijing, 100029, China

Abstract

Sulfur trioxide (SO₃) is one of the most active chemical species in the atmosphere, and its atmospheric fate has profound implications to air quality and human health. The dominant gas-phase loss pathway for SO₃ is generally believed to be the reaction with water molecules, resulting in sulfuric acid. The latter is viewed as a critical component in the new particle formation (NPF). Herein, a new and competitive loss pathway for SO₃ in the presence of abundant gas-phase ammonia (NH₃) species is identified. Specifically, the reaction between SO₃ and NH₃, which produces sulfamic acid, can be self-catalyzed by the reactant (NH₃). In dry and heavily polluted areas with relatively high concentrations of NH₃, the effective rate constant for the bimolecular SO₃-NH₃ reaction can be sufficiently fast through this new loss pathway for SO₃ to become competitive with the conventional loss pathway for SO₃ with water. Furthermore, this study shows that the final product of the reaction, namely, sulfamic acid, can enhance the fastest possible rate of NPF from sulfuric acid and dimethylamine by about a factor of two. An alternative source of stabilizer for acid-base clustering in the atmosphere is suggested, and this new mechanism for NPF has implication to improved atmospheric modeling in highly polluted regions.

1. Introduction

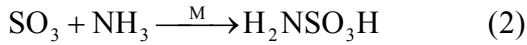
Sulfur trioxide (SO_3) is a major air pollutant¹⁻⁵ and is mainly produced by the gas-phase oxidation of SO_2 ⁶⁻⁷. As a highly reactive gas⁸ and one of the most common acid oxides, SO_3 can lead to both acid rain and atmospheric aerosol⁹⁻¹³ and thus has important implications for regional climate and human health¹⁴⁻¹⁹. The reaction between SO_3 and water (H_2O) has been generally considered as the dominant pathway for the loss of SO_3 because the H_2O concentration is $\sim 10^{17}$ molecules cm^{-3} in the boundary layer, which is several orders of magnitudes greater than that of other condensable gases.²⁰ The relevant reaction equation can be described by the reaction (1):



Both experimental and theoretical studies²¹⁻²⁶ indicate that a facilitator molecule M, acting as a catalyst, is required. For example, previous experiment study by Jayne et al.²³ showed that the reaction (1) exhibits second-order dependence on water vapor concentration, and other previous theoretical studies²² indicated the addition of a second water molecule could substantially lower the activation barrier. More recently, sulfuric acid (SA)²⁴ or other atmospheric molecules (such as formic acid²⁵ or ammonia²⁶) make the reactions barrierless and thus significantly fast. However, in highly polluted regions, the concentration of NH_3 can reach $105.0 \mu\text{g m}^{-3}$ (or $\sim 3.7 \times 10^{12}$ molecules cm^{-3})²⁷. Furthermore, in relatively dry conditions or at lower temperatures, e.g., in the winter, the concentration of gas-phase water molecules is drastically reduced.¹³ Hence, SO_3 may react with NH_3 before reacting with H_2O .

The possibility of an $\text{SO}_3\text{-NH}_3$ reaction was previously studied in the laboratory, and its effective rate coefficient was detected to be $10^{-12}\text{-}10^{-10} \text{ cm}^3 \text{ molecule}^{-1}\text{s}^{-1}$ at NH_3 concentration of $10^{11}\text{-}10^{13}$ molecules cm^{-3} ²⁸⁻³². Such unexpectedly high values of the rate coefficient are similar to those of SO_3 and water dimer reaction ($10^{-11}\text{-}10^{-10} \text{ cm}^3 \text{ molecule}^{-1} \text{ s}^{-1}$)^{21-23,33}, implying that the reaction with NH_3 might be an important sink of SO_3 . A Fourier-transform infrared spectroscopy (FTIR) study by Hirota et al.³⁰ showed that with NH_3 , the product from the reaction of SO_3 is sulfamic acid

(H₂NSO₃H, SFA). Previous theoretical studies³⁴⁻³⁵ predicted that a direct SO₃-NH₃ reaction is kinetically unfavorable because of the high reaction barrier (28.6 kcal/mol). The discrepancy between theoretical and experimental results suggests that this reaction might require a facilitator molecule M, as in reaction (2):



Thus, it is important to determine whether reaction (2) entails a much lower reaction barrier with either another NH₃ molecule or the SFA molecule as a catalyst, and also important to elucidate the underlying reaction mechanism.

From the perspective of its structure, SFA possesses two functional groups: a sulfonic acid and an amino group. Both groups can act as hydrogen donors and acceptors to interact with atmospheric particle precursors as proven by previous works³⁶⁻³⁹. Furthermore, in the experiment performed by Lovejoy et al.²⁹, SFA was observed to cluster efficiently with itself and SA, indicating its potential for aerosol new particle formation (NPF). Although several compounds have been identified in promoting NPF process, they are mostly correlated with special environment, for example, highly oxidized multifunctional organic molecules (HOMs) mostly in forest, rural and urban areas⁴⁰⁻⁴³, iodic acid (HIO₃) in coastal area and open ocean region⁴⁴, and methanesulfonic acid (MSA) mostly in marine region⁴⁵. A main question that we intend to address here is whether SFA produced by the reaction between SO₃ and NH₃ is capable of enhancing the nucleation of SA and base (i.e., ammonia or amine) molecular clusters, in view of that the latter species have been recognized as dominant precursors in highly polluted areas, especially in some megacities in Asia⁴⁶⁻⁵³.

In this work, using high-level theoretical methods, we first studied the reaction between SO₃ and NH₃ to form SFA with the reactant (NH₃) or product (SFA) being considered as a self- or auto-catalyst. Next, we used the Atmospheric Clusters Dynamic Code (ACDC)⁵⁴ to investigate how the product (SFA) is involved in SA-dimethylamine (SA-DMA)-based cluster formation. Particular attention of this work is placed on the study of 1) the possibility of the SO₃ and NH₃ reaction

functioning as an important loss pathway in highly polluted areas with high NH₃ concentrations and 2) the fate of the product in atmospheric NPF and the influence of various environmental conditions.

2. Methods

Quantum Chemical Calculation. All density functional theory (DFT) calculations were performed with using Gaussian 09⁵⁵ software packages. For all reactions involving SO₃ and NH₃, structure optimization and subsequent frequency analysis of the stationary points were carried out at the M06-2X/6-311++G(3df,3pd) level of theory. Several previous studies^{36-39,56} have shown that the M06-2X meta functional is an accurate DFT method for computing thermochemistry, kinetics and noncovalent interactions involving the main-group elements. Intrinsic reaction coordinate (IRC) was also calculated to assure the correct transition states for the products and reactants. Single-point energies for the stationary points were computed using the ORCA 3.03 Package⁵⁷ to obtain more reliable energies. To this end, the explicitly correlated coupled cluster (CCSD(T)-F12)⁵⁸ method with the cc-pVDZ-F12 basis set⁵⁹ and appropriate auxiliary basis sets were used.

For the chemical processes involving interactions between SFA and other precursors resulting in particle formation, a systematic sampling technique was used to search for the global minima of the molecular clusters. In the first step, a thousand structures are auto-generated using the ABCluster⁶⁰ software with the TIP4P⁶¹⁻⁶² model for water molecules and the CHARMM⁶³ force field for others; these structures were then pre-optimized based on the semi-empirical method (PM7) with Mopac2016⁶⁴⁻⁶⁵. Next, up to 100 low-energy conformations were re-optimized using the M06-2X/6-31+G* level of theory to determine the ten lowest-lying structures, followed by another optimization with using the larger 6-311++G(3df,3pd) basis set to determine the global minimum. The Cartesian coordinates and the corresponding formation Gibbs free energy of the stable clusters are summarized in the Supporting Information.

Atmospheric Clusters Dynamic Code (ACDC) model. The ACDC⁵⁴ kinetic model

with the MATLAB-R2013a⁶⁶ program is used to compute the time evolution of formation rates and growth paths of the clusters. For a given set of atmospheric clusters, the code can be used to solve the birth-death equations (see equation (3) below) with calculated formation free energies (based on other theoretical method) as the inputs. The overall process accounts for all possible collision and evaporation of the relevant clusters. Specifically, the birth-death equation is written as

$$J = \frac{dc_i}{dt} = \frac{1}{2} \sum_{j < i} \beta_{j,(i-j)} c_j c_{(i-j)} + \sum_j \gamma_{(i+j) \rightarrow i} c_{i+j} - \sum_j \beta_{i,j} c_i c_j - \frac{1}{2} \sum_{j < i} \gamma_{i \rightarrow j} c_i + Q_i - S_i \quad (3)$$

where J refers to the cluster formation rate, i (or j) is a molecule or a cluster, c_i stands for the concentration of i , $\beta_{i,j}$ or $\gamma_{i+j \rightarrow i}$ are the collision coefficient of i with j or the evaporation coefficient of $i+j$ cluster evaporating into i and j , respectively. Q_i , set to be zero in the present study, is the possible other source of i . S_i represents the sink term of i .

The collision coefficient $\beta_{i,j}$ is based on the kinetic gas theory⁶⁷⁻⁶⁸ and equation (4):

$$\beta_{i,j} = \left(\frac{3}{4\pi}\right)^{1/6} \left(\frac{6k_b T}{m_i} + \frac{6k_b T}{m_j}\right)^{1/2} (V_i^{1/3} + V_j^{1/3})^2 \quad (4)$$

where m_i and V_i are the mass and volume of i , and similarly, m_j and V_j are the mass and volume of j , respectively, which are calculated via the following formula (5):

$$V = \left(\frac{4}{3}\right) \times \pi \times (r)^3 \quad (5)$$

where r is the molecular radius derived by using Multiwfn software⁶⁹. More details can be found from our previous paper⁷⁰.

The evaporation coefficient $\gamma_{i+j \rightarrow i}$ was calculated using the formation Gibbs free energies of the given clusters and equation (6):

$$r_{(i+j) \rightarrow j} = \beta_{i,j} \frac{c_i^e c_j^e}{c_{i+j}^e} = \beta_{i,j} C_{ref} \exp\left\{\frac{\Delta G_{i+j} - \Delta G_i - \Delta G_j}{k_b T}\right\} \quad (6)$$

where c_i^e refers to the equilibrium concentration of i , ΔG_i is the formation free energy of i , and C_{ref} represents the monomer concentration of the reference vapour at a pressure of 1 atm, which is the pressure at which the Gibbs free energies are determined.

Generally, the simulation system is regarded as an “ $a \times b$ ” box, where a or b is the maximum number of acid or base molecules of the clusters, respectively. Here, the cluster size of the simulated systems was set to be 3×2 , containing $(SFA)_x(SA)_y(DMA)_z$ (where the sum of x and y from 0 to 3, z from 0 to 2) clusters. The mobility diameter of the largest cluster is 1.7 nm which is chosen because the NPF rates typically use this standard during experimental measurement.⁷¹ Among these clusters, only the clusters including an equal numbers of base and acid molecules or the clusters with smaller numbers of base than acid molecules were considered, as only these clusters have the potential to further grow into larger sizes.⁷¹ In addition, considering the formation Gibbs free energy (Table S1) and evaporation rates (Table S2), the clusters containing SA and DMA molecules and an SFA molecule are the most stable and are therefore allowed to grow to larger clusters, thereby contributing to the rate of NPF. Given the above considerations, clusters $(SA)_3 \cdot (DMA)_3$ and $SFA \cdot (SA)_2 \cdot (DMA)_3$ are set as the boundary clusters. Moreover, the coagulation sink coefficient is set to be $5 \times 10^{-2} \text{ s}^{-1}$ in the case of polluted areas.⁷³⁻⁷⁵

3. Results and Discussion.

Reactant as self-catalyst and product as auto-catalyst. A previous theoretical study³⁴ showed that the direct reaction between SO_3 and NH_3 without a catalyst is not a plausible path for SFA formation due to a high reaction barrier (Figure 1(a)). The high barrier is a consequence of large ring tension of the rather closed four-membered-ring transition-state geometry, making SFA formation kinetically

unfavorable. However, experimental studies^{28,29} have indicated that the bimolecular rate coefficient for the SO₃-NH₃ reaction can reach ~10⁻¹⁰ cm³ molecule⁻¹ s⁻¹. Such a high reaction rate coefficient reflects a fast and easy reaction. The apparent inconsistency between experimental results and theoretical prediction indicates that the reaction between SO₃ and NH₃ may involve a catalyst. Thus, we first examine the SFA formation from the SO₃ and NH₃ reaction with either the NH₃ reactant or the SFA product as a catalyst. As shown in Figure 1(b), with the reactant (NH₃) acting as a catalyst, the reaction barrier is substantially lower than that of the direct reaction (Figure 1(a)). Reactions starting with the formation of different dimers among two of three molecules (SO₃, NH₃ and NH₃ molecules) were examined, and we expected the SO₃·NH₃ heterodimer to be the best candidate due to its most negative Gibbs free energy of formation (-10.0 kcal mol⁻¹) among the possible dimers. Next, the reaction continues to yield a pre-reactive complex C2 with a formation free energy of -12.4 kcal mol⁻¹, followed by the formation of a hydrogen-bonded complex P2 via TS2 transition state, with a free energy barrier of 5.7 kcal mol⁻¹. The NH₃ molecule in TS2 acts as a double donor and a single acceptor of hydrogen to form a steric network with an SO₃·NH₃ heterodimer through van der Waals interactions. As a result, the ring strain of the transition state is reduced with increasing ring size from a four-membered ring structure to a cage-like hydrogen-bonding network; the associated energy barrier is significantly lower than that without the self-catalyst. Hence, the reactant self-catalysis mechanism for the SO₃-NH₃ reaction is predicted.

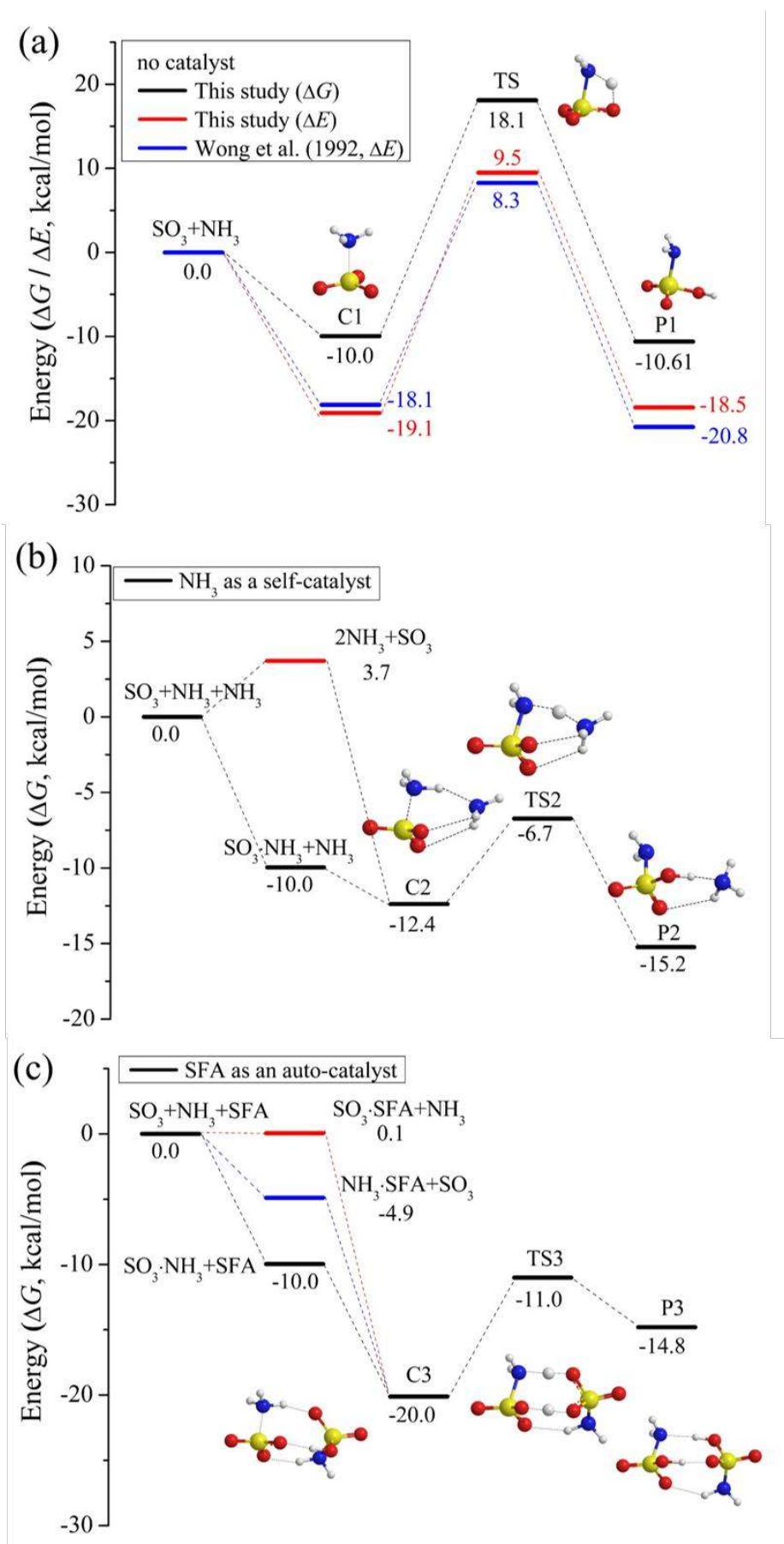
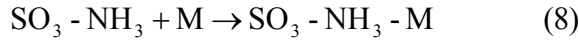
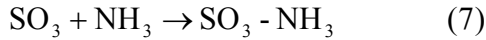


Figure 1. Potential energy surfaces for the reaction of SO₃ and NH₃ with (a) no catalyst; (b) NH₃ as a self-catalyst; and (c) SFA as an auto-catalyst. Hydrogen, oxygen, sulfur, and nitrogen atoms are represented by gray, red, yellow and blue spheres, respectively.

In addition to reactant (NH₃) self-catalysis mechanism, the SFA auto-catalysis mechanism (Figures 1(c)) can also facilitate the formation of SFA with high efficiency. The reaction barrier involved is 9.0 kcal mol⁻¹, which is also much lower than that without the auto-catalyst (Figures 1(a)). This auto-catalysis reaction can, in principle, begin with three primary paths involving either the bimolecular collision between an NH₃ molecule and an SO₃ molecule, a collision between an SO₃ molecule and an SFA molecule, or a collision between an SFA molecule and an NH₃ molecule. However, Figure 1(c) shows that the first path is most likely due to the greater stability of SO₃ · NH₃ heterodimer among the three possible firstly formed dimers. Thus, the reaction starting with the formation of an SO₃ · NH₃ heterodimer, followed by the formation of a pre-reactive complex C3, with a formation free energy of -20.0 kcal mol⁻¹ (much lower than the value for C2 (-12.4 kcal mol⁻¹)) indicates greater binding ability of the SO₃ · NH₃ heterodimer with product SFA than with reactant NH₃. Finally, the complex C3 proceeds via transition state TS3 to form a hydrogen-bonding complex P3. In the mechanism above, the product SFA molecule, as an auto-catalyst, mediates the formation of the N-S covalent bond by transfer a proton from NH₃ to an oxygen atom of SO₃. These computations indicate that either the reactant or product can function as a catalyst to make the reaction between SO₃ with NH₃ much more energetically accessible, as observed in previous experiments.

Reaction rate of the SO₃-NH₃ reaction. Given the self-catalysis ability of reactant NH₃ and the auto-catalysis ability of product SFA, it is important to examine the reaction rate of the SO₃ and NH₃ reaction and compare this rate with that of the SO₃ and H₂O reaction to determine if the reaction with NH₃ is an important loss pathway

for SO_3 . Kinetic calculations are carried out based on conventional transition-state theory (TST)^{24-25, 76-78} to evaluate the effects of NH_3 and SFA on the rate constants for the reaction between SO_3 and NH_3 . Besides, the TST with Wigner tunneling correction is also considered (see Table S3) and the results indicate that the tunneling effect has little impact on the reaction rate constant. As previously described, the self- or auto-catalyzed reaction mainly proceeds via the following reaction sequence:



where M represents the catalyst (reactant NH_3 or product SFA). The energy profiles for reaction steps (7)-(10) shown in Figure 1(b)-(c) indicates that reaction (9) is the rate-determining step. Applying the steady-state approximation to the pre-reactive complex and assuming that the complex is in equilibrium with the reactant, we derive the following equation:

$$r = \frac{d[\text{SFA}]}{dt} = \frac{k_7}{(k_{-7} + k_8[\text{M}])} \times \frac{k_8}{(k_{-8} + k_9)} \times k_9 [\text{SO}_3][\text{NH}_3][\text{M}] \quad (11)$$

where k_7/k_{-7} and k_8/k_{-8} denote the ratio of the forward/reverse rate coefficients for reactions (7) and (8), respectively, and k_{10} is the unimolecular rate constant for reaction (9). Thus, the rate constant k for reaction (2) can be expressed as

$$k = \frac{r}{[\text{SO}_3][\text{NH}_3]} = \frac{k_7}{(k_{-7} + k_8[\text{M}])} \times \frac{k_8}{(k_{-8} + k_9)} \times k_{10}[\text{M}] \quad (12)$$

where k can be viewed as a measure of the relative efficiency of different catalysts because their concentrations are also included in equation (12).

For SFA concentration, wide ranges from 10^{11} to 10^{15} molecules cm^{-3} and from 10^4 to 10^8 molecules cm^{-3} are examined, respectively, corresponding to an SO_3

concentration of 10^9 - 10^{13} molecules cm^{-3} considered in the laboratory and a concentration of 10^0 - 10^5 molecules cm^{-3} observed in the atmosphere (see Tables S4 and S5). The computed rate constants for both conditions are presented in Table 1. Without considering the catalyst, the rate constant k is $\sim 10^{-20}$ $\text{cm}^3 \text{ molecule}^{-1} \text{ s}^{-1}$, which is too small for the reaction to occur. Under typical laboratory conditions, the reaction rate constant k for the SO_3 and NH_3 reaction catalyzed by either reactant NH_3 or product SFA increases significantly and the rate constant can be as high as 10^{-10} $\text{cm}^3 \text{ molecule}^{-1} \text{ s}^{-1}$, consistent with the experimentally measured value²⁸⁻²⁹. Both reactant self-catalysis and product auto-catalysis mechanisms can explain the observed spectral signals of SFA formed from SO_3 (in the presence of SO_2 and O_2) and NH_3 in the laboratory.³⁰ However, considering that the product SFA concentration is significantly lower than that observed in the experiment (10^4 to 10^8 molecules cm^{-3} in Table S5), the high reaction rate constant (10^{-10} $\text{cm}^3 \text{ molecule}^{-1} \text{ s}^{-1}$) would be difficult to attain through SFA auto-catalysis alone. Thus, we expect that the reaction through NH_3 self-catalysis is the major sink of SO_3 in areas with abundant NH_3 in the atmosphere.

The competition between the two reactions, one between SO_3 and NH_3 and the other between SO_3 and H_2O , also warrants investigation given that the latter reaction is generally considered as the dominant loss process of SO_3 . The rate constant of the SO_3 and $(\text{H}_2\text{O})_2$ reaction is 10^{-11} - 10^{-10} $\text{cm}^3 \text{ molecule}^{-1} \text{ s}^{-1}$ for H_2O -involved self-catalysis reaction²⁶. Under normal atmospheric conditions, the concentration of $(\text{H}_2\text{O})_2$ ($\sim 10^{14}$ molecules cm^{-3})⁷⁹⁻⁸⁰ is much higher than that of NH_3 ; hence, the reaction with H_2O will be the dominant sink pathway for SO_3 . However, in highly polluted areas with relatively dry conditions, the concentration of NH_3 can be comparable with that of $(\text{H}_2\text{O})_2$; thus, the reaction between SO_3 and NH_3 can potentially compete with the reaction between SO_3 and H_2O (ratios of the rates of the two reactions are given in Tables S6-S9). Note also that Bandyopadhyay et al.²⁶ suggested that the $\text{SO}_3 + \text{H}_2\text{O}$ reaction can also be effectively catalyzed by NH_3 molecule, with a high reaction rate constant ($\sim 10^{-4}$ $\text{cm}^3 \text{ molecule}^{-1} \text{ s}^{-1}$) for SO_3 and

$\text{H}_2\text{O}\cdot\text{NH}_3$ reaction. Given that the $\text{H}_2\text{O}\cdot\text{NH}_3$ concentration is several orders of magnitude lower than that of $(\text{H}_2\text{O})_2$ or NH_3 , the reaction of SO_3 and NH_3 could also be competitive with that of SO_3 and $\text{H}_2\text{O}\cdot\text{NH}_3$ (ratios of the rates of the two reactions are given in Tables S10-S12).

Table 1. Calculated forward/reverse rate coefficients (k_7/k_{-7} and k_8/k_{-8}), the unimolecular rate constant (k_9), the concentration of catalyst ($[\text{M}]$), and the reaction rate constant (k) for the reaction of $\text{SO}_3 + \text{NH}_3$ without a catalyst, with reactant NH_3 as a self-catalyst and the product SFA as an auto-catalyst.

	Without catalyst	NH ₃ self-catalysis	SFA auto-catalysis (under laboratory conditions)	SFA auto-catalysis (under atmospheric conditions)
$k_7 (\text{cm}^3 \text{molecule}^{-1} \text{s}^{-1})$	4.35×10^{-10}	4.35×10^{-10}	4.35×10^{-10}	4.35×10^{-10}
$k_{-7} (\text{s}^{-1})$	5.32×10^2	5.32×10^2	5.32×10^2	5.32×10^2
$k_8 (\text{cm}^3 \text{molecule}^{-1} \text{s}^{-1})$	----	4.96×10^{-10}	3.96×10^{-10}	3.96×10^{-10}
$k_{-8} (\text{s}^{-1})$	----	1.99×10^8	4.12×10^2	4.12×10^2
$k_9 (\text{s}^{-1})$	1.64×10^{-8}	4.46×10^8	1.53×10^6	1.53×10^6
$[\text{M}]$ (molecules cm^{-3})	-----	$10^9\text{-}10^{13}$	$10^{11}\text{-}10^{15}$	$10^4\text{-}10^8$
$k (\text{cm}^3 \text{molecule}^{-1} \text{s}^{-1})$	1.33×10^{-20}	$2.78 \times 10^{-13} \text{ to } 2.72 \times 10^{-10}$	$3.01 \times 10^{-11} \text{ to } 4.34 \times 10^{-10}$	$3.23 \times 10^{-18} \text{ to } 4.34 \times 10^{-14}$
effective rate constant ²⁸⁻²⁹		$10^{-12}\text{-}10^{-10} (\text{cm}^3 \text{molecule}^{-1} \text{s}^{-1})$ (laboratory conditions)		

Atmospheric Implication: Enhancement Effect of SFA on NPF

Knowing that the formation of SFA becomes an important and competitive loss pathway for SO₃ in the atmosphere with a high concentration of NH₃, we performed ACDC simulations to achieve a deeper understanding of the influence of SFA on SA-DMA-based molecular clustering, a known source for NPF. The ratio (r_{SFA}) of formation rates with SFA to the rate without SFA is given by equation (12) for temperature $T = 298, 278, 258$ K, corresponding to the temperature conditions in the boundary layer and in the lower troposphere⁸¹:

$$r_{\text{SFA}} = \frac{J([\text{SFA}] = x, [\text{SA}] = y, [\text{DMA}] = z)}{J([\text{SA}] = y, [\text{DMA}] = z)} \quad (12)$$

where [SFA], [SA] and [DMA] stand for SFA, SA and DMA concentration, respectively. [SFA] was varied from 10^4 to 10^8 molecules cm⁻³ (Table S5); the 10^4 - 10^8 molecules cm⁻³ of [SA], and 10^7 - 10^{11} molecules cm⁻³ of [DMA] are chosen, since these values are the typical observed values in the atmosphere⁸²⁻⁸⁴. The enhancement factor (r_{SFA}) at three different temperatures (Tables S14-S16, Figures S1-S2 and Figure 2) is always equal to or larger than 1.0, reflecting the enhancement ability of SFA on the SA-DMA-based system. At 278K, for example, the dependence of the enhancement factor r_{SFA} on [SFA], [SA] and [DMA] is shown in Figure 2. The r_{SFA} increases with increasing [SFA] and reaches as high as 10^5 at [SFA] = 10^8 molecules cm⁻³ (Figure 2(a) and (b)) with low [SA] of 10^4 molecules cm⁻³. Generally, high absolute cluster formation rates relevant to observed atmospheric NPF^{46, 50,84-85} are associated with fairly low values of r_{SFA} (Tables S14-S16). However, the enhancement effect of SFA may still be significant in many atmospherically relevant conditions - for example at [SA] = 10^6 and [DMA] = 10^{10} molecules cm⁻³, an SFA concentration of 10^6 leads to an enhancement factor of 2 at $T = 298$ K and an overall formation rate of $J = 115$ cm⁻³ s⁻¹.

Moreover, r_{SFA} decreases as [SA] increases, as shown in Figure 2(a), likely due to the stronger binding between SA and DMA than between SFA and DMA (or between

SFA and SA). At a constant concentration of SFA and DMA, increasing SA leads to increased SA-DMA clustering at the expense of SFA-containing clusters and to decreased r_{SFA} , even as the overall particle formation rate increases. The influence of [DMA] on the ratio r_{SFA} shows different trend compared with that of [SA] (Figure 2(b)), where r_{SFA} increases firstly as [DMA] changes from 10^7 to 10^{10} molecules cm^{-3} . This might be due to the increased hydrogen bonding interaction between acidic molecule SFA and the added base molecule DMA. As such, with the increase of [DMA] to 10^9 molecules cm^{-3} , saturation of hydrogen bonding interaction is reached for SFA, thus resulting in the maximum enhancement strength. Whereas, with further increase of [DMA], r_{SFA} decreases as [DMA] changes from 10^{10} to 10^{11} molecules cm^{-3} . This is because the hydrogen bonds between SFA and SA could be disrupted by the added DMA molecules, leading to the decreased interaction between SFA with other molecules, thereby decreasing the r_{SFA} . This phenomenon could be a common feature for the system involving acidic compounds, such as HMSA and glycolic acid.^{37, 86} Furthermore, the variation of enhancement factor with the increase of [DMA] in the presence of NH_3 is further examined (Figure S3). The results show that enhancement factor of SFA first increases and then decreases with increasing [DMA], while the common $[\text{NH}_3]$ of 10^{10} to 10^{11} molecules cm^{-3} has only a minor effect.

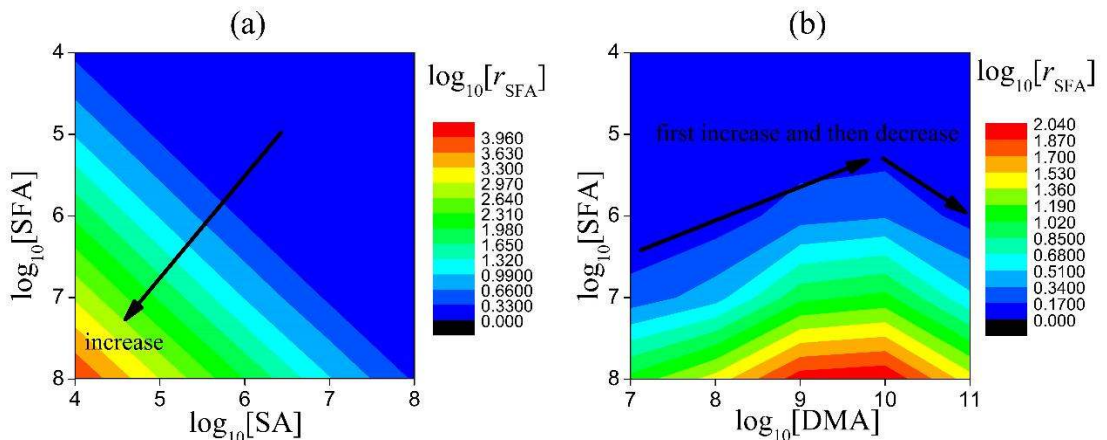


Figure 2. (a) The cluster formation rates ratio (r_{SFA}) versus the logarithm of [SA] and [SFA] at $[\text{DMA}] = 10^9$ molecules cm^{-3} and (b) the cluster formation rates ratio (r_{SFA}) versus the logarithm of [DMA] and [SFA] ($T = 278$ K and $10^4 \leq [\text{SFA}] \leq 10^8$ molecules cm^{-3}).

To further identify the mechanism by which SFA offers its enhancement effect, the main pathways of cluster growth were traced using ACDC. The principal growth paths of SFA-SA-DMA-based clusters at different [SFA] with median [SA] of 10^6 molecules cm^{-3} and [DMA] of 10^9 molecules cm^{-3} at 278 K are shown in Figure 3. At $[\text{SFA}] = 10^4$ and 10^5 molecules cm^{-3} , SFA molecules do not substantially contribute to the cluster growth, and the pathway just shows the growth of pure SA-DMA-based clusters. These results are consistent with those in Figure 2(a), where SFA also shows no effect on cluster formation rate. When $[\text{SFA}]$ is increased to 10^6 molecules cm^{-3} , SFA appears to be responsible for an alternative pathway (marked by blue lines in Figure 3). In this pathway, the initially generated SFA-containing cluster is $\text{SFA}\cdot\text{SA}\cdot\text{DMA}$, formed by collision of SFA with a pre-existing $\text{SA}\cdot\text{DMA}$ cluster. Thereafter, the $\text{SFA}\cdot\text{SA}\cdot\text{DMA}$ cluster grows via a base-stabilization mechanism, and each addition of an acid molecule is stabilized by one additional DMA molecule, following the sequence of acid-base pairs: $\text{SFA}\cdot\text{SA}\cdot\text{DMA} \rightarrow \text{SFA}\cdot\text{SA}\cdot(\text{DMA})_2 \rightarrow \text{SFA}\cdot(\text{SA})_2\cdot(\text{DMA})_2 \rightarrow$ flux out. In this case, the contribution of SFA is only 10%. While, with the further increase of $[\text{SFA}]$, its role becomes even more important. As shown in Figure 3, SFA plays a dominant role, and its contribution is substantially increased from 10% at $[\text{SFA}] = 10^6$ molecules cm^{-3} to 50% at $[\text{SFA}] = 10^7$ molecules cm^{-3} .

SFA molecule shows an ability to directly participate in cluster formation, suggesting that SFA can be a “participator” in facilitating NPF. Contrary to other common acid species as reported in our recent works^{70,87,88}, such organic acids, e.g., lactic acid and glyoxylic acid, and inorganic acid, e.g., nitric acid, can only be indirectly involved in the growth pathway, acting as a “transporter” (which initially participates and eventually evaporates). Note that like SFA, another two species with sulfonic group, namely, methanesulfonic acid (MSA)³⁶ and hydroxymethanesulfonic acid (HMSA)³⁷, are also identified to directly participate in the cluster formation. However, depending on the formation source of these species, the MSA tends to promote NPF mainly on marine areas. Although HMSA is likely to participate in the

process of NPF³⁷, the formation source of HMSA in the gas phase is still an open question and its atmospheric concentration still needs to be explored to confirm its roles in NPF. Overall, among the three splices containing sulfonic groups, the SFA represents the most compiling species towards NFP in highly polluted areas with high NH₃ concentration.

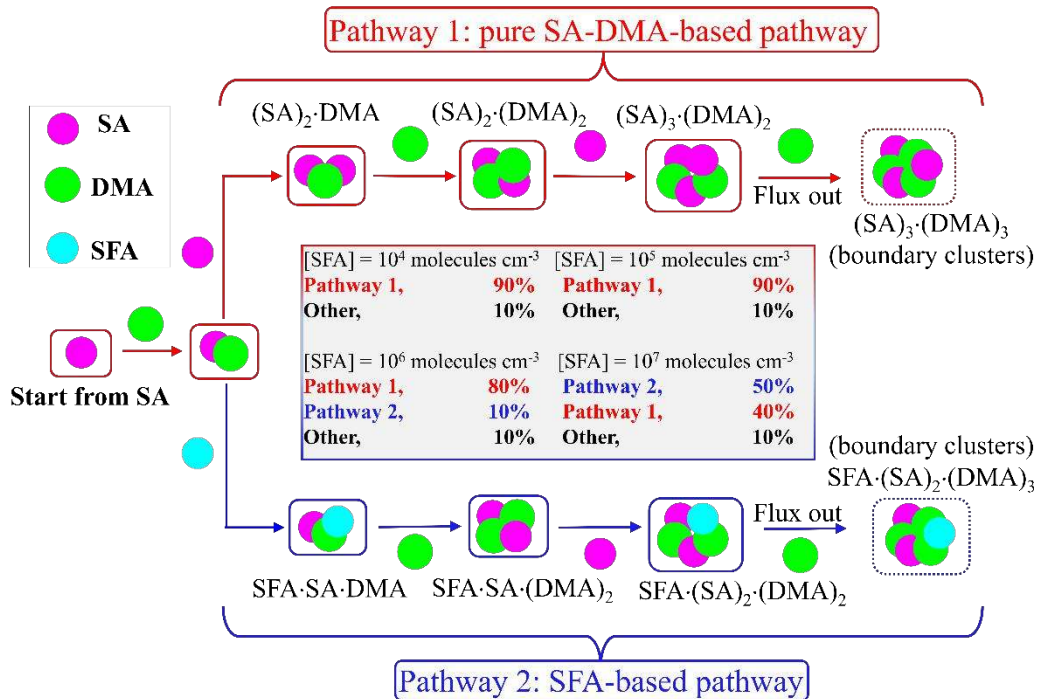
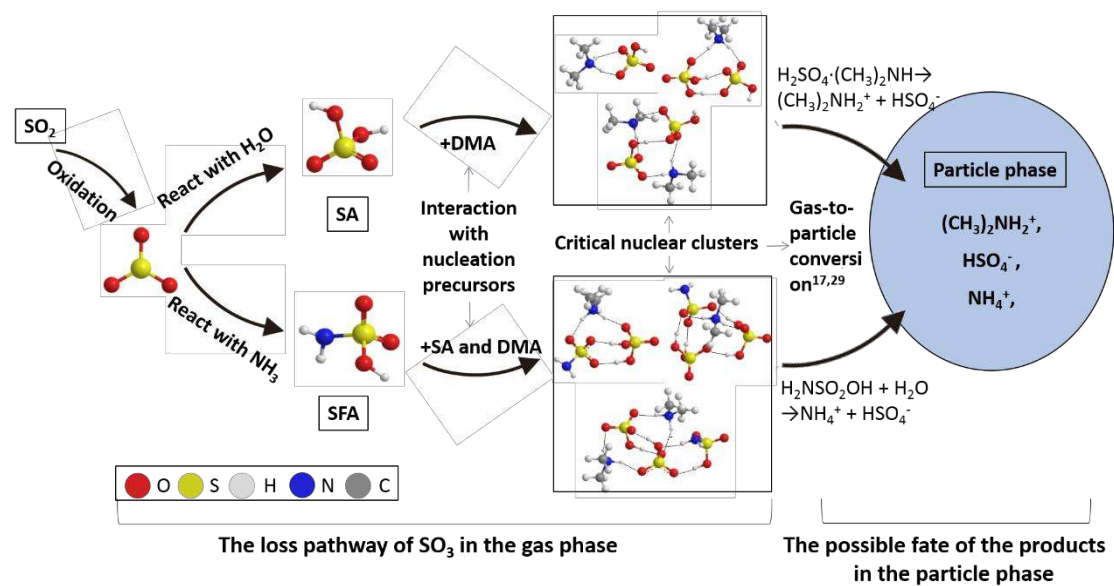


Figure 3. Main pathways and the corresponding mechanism of cluster growth within the cluster size range considered, at $T = 278\text{K}$, $[\text{SA}] = 10^6 \text{ molecules cm}^{-3}$, $[\text{DMA}] = 10^9 \text{ molecules cm}^{-3}$ and $10^4 \leq [\text{SFA}] \leq 10^8 \text{ molecules cm}^{-3}$. The blue and red fluxes represent the growth pathways of SFA-contained clusters and pure SA-DMA-based clusters, respectively.

The environmental fate of SFA is likely to hydrolyze to ammonium sulfate in the aqueous phase, as previously reported³⁰⁻³¹. Thus, the formation of SFA-containing molecular clusters, followed by reaction with water and hydrolysis to form ammonium sulfate, may constitute an alternate pathway to sulfate production in the particle phase (see Scheme 1). All the suggested mechanisms may also be extended to

the other loss paths of SO_3 with other common bases, such as amines, which are also likely to contribute to the atmospheric sink of SO_3 , especially in areas with high concentrations of the base gases. Hence, scenarios involving SFA and its analogues should be assessed on their role in atmospheric particle formation.

Scheme 1. A suggested scheme of the important loss pathway for SO_3 in highly polluted atmosphere with a high NH_3 concentration.



5. Conclusion

We have investigated the reaction of NH_3 with SO_3 to form SFA and the subsequent effect of SFA on NPF in highly polluted regions with high concentration of NH_3 . The important chemistry found in this study is that, with self-catalysis by the reactant NH_3 , the activation barrier for the $\text{SO}_3\text{-NH}_3$ reaction can be drastically lowered. Hence, at high NH_3 concentration, the effective reaction rate coefficient can reach $\sim 10^{-10} \text{ cm}^3 \text{ molecule}^{-1}\text{s}^{-1}$, which indicates that the reaction is sufficiently fast to be competitive with the conventional $\text{SO}_3\text{-H}_2\text{O}$ reaction (effective rate constant of $10^{-11}\text{-}10^{-10} \text{ cm}^3 \text{ molecule}^{-1}\text{s}^{-1}$). This newly identified self-catalyzed reaction provides a previously unreported loss pathway of SO_3 at relatively low H_2O concentration and high NH_3 concentration. Our study shows that the product of the self-catalyzed reaction, SFA, can directly participate in the SA-DMA-based cluster formation, thereby substantially

enhancing the cluster formation rate. This new stabilization mechanism in acid-base clustering has important implication to the aerosol NPF in highly polluted regions with high concentrations of base species.

ASSOCIATED CONTENT

Supporting Information

The Supporting Information is available free of charge on the ACS Publications website. Tables S1-S2 give the formation Gibbs free energies and the sum of evaporation rates of the clusters, respectively. Table S3 give the imaginary frequencies of the transition states (TSs) and the Wigner tunneling correction factor (Γ) of the reactions. Tables S4-S5 give the possible concentration of SFA in the experiment and in the real atmosphere, respectively. Tables S6-S12 give the ratio of reaction rate for $\text{SO}_3 + \text{NH}_3$ reaction and $\text{SO}_3 + \text{H}_2\text{O}$ reaction under different $[\text{NH}_3]$ and $[\text{H}_2\text{O}]$. Table S13 gives the formation Gibbs free energies (ΔG) and a sum of evaporation rates of the clusters containing SFA, SA DMA and NH_3 at 278K. Tables S14-S16 give the enhancement strength of SFA in the case of $10^4 \leq [\text{SA}] \leq 10^8$ molecules cm^{-3} , $10^7 \leq [\text{DMA}] \leq 10^{11}$ molecules cm^{-3} , $10^4 \leq [\text{SFA}] \leq 10^8$ molecules cm^{-3} at three different temperatures (298, 278 and 258K), respectively. Figures S1-S2 give the ratio of cluster formation rates as a function of the logarithm of [SA] and [DMA] at $T = 298$ and 258 K, respectively. Optimized geometries of key species involved in particle formation in gas-phase are also provided. Figure S3 gives the ratio of cluster formation rates versus the logarithm of [DMA].

Acknowledgements

We thank the Chinese National Natural Science Foundation (91544227, 21373025), and “the Fundamental Research Funds for the Central Universities”. We also gratefully thank the useful help of Jonas Elm (Aarhus University). Hao Li thanks CSC (China Scholarship Council). T.K. thanks the Academy of Finland for funding. H.V. thanks the European Research Council (Grant 692891-DAMOCLES) and the University of Helsinki, Faculty of Science ATMATH project for funding. We also

thank computation support of UNL Holland Computing Center.

AUTHOR INFORMATION

Authors contribute equally.

Corresponding Authors

*Email: zhangxiuhui@bit.edu.cn

*Email: jfrancisco3@unl.edu

*Email: xzeng1@unl.edu

References

1. Zhuang, Y.; Pavlish, J. H. *Environ. Sci. Technol.* **2012**, *46*, 4657.
2. Chen, L.; Bhattacharya, S. *Environ. Sci. Technol.* **2013**, *47*, 1729.
3. Cao, Y.; Zhou, H.; Jiang, W.; Chen, C.; Pan, W. *Environ. Sci. Technol.* **2010**, *44*, 3429.
4. Kikuchi, R. *Environ. Manage.* **2001**, *27*, 837.
5. Mitsui, Y.; Imada, N.; Kikkawa, H.; Katagawa, A. *Int. J. Greenh. Gas. Con.* **2011**, *5*, S143.
6. Stockwell, W. R.; Calvert, J. G. *Atmos. Environ.* **1983**, *17*, 2231.
7. Mauldin III, R. L.; Berndt, T.; Sipilä, M.; Paasonen, P. *Nature* **2012**, *488*, 193.
8. Fleig, D.; Vainio, E.; Andersson, K.; Brink, A.; Johnsson, F.; Hupa, M. *Energy & Fuels* **2012**, *26*, 5537.
9. Sipilä, M.; Berndt, T.; Petäjä, T.; Brus, D.; Vanhanen, J.; Stratmann, F.; Patokoski, J.; Hyvärinen, A. P.; Lihavainen, H. *Science* **2010**, *327*, 1243.
10. Mackenzie, R. B.; Dewberry, C. T.; Leopold, K. R. *Science* **2015**, *349*, 58.
11. England, G. C.; Zielinska, B.; Loos, K.; Crane, I.; Ritter, K. *Fuel. Process. Technol.* **2000**, *65–66*, 177.
12. Li, L.; Kumar, M.; Zhu, C.; Zhong, J.; Francisco, J. S.; Zeng, X. C. *J. Am. Chem. Soc.* **2016**, *138*, 1816.

13. Renard, J. J.; Calidonna, S. E.; Henley, M. V. *J. Hazard. Mater.* **2004**, *108*, 29.
14. Zhang, R.; Khalizov, A.; Wang, L.; Hu, M.; Xu, W. *Chem. Rev.* **2012**, *112*, 1957.
15. Pöschl, U. *Angew. Chem. Int. Edit.* **2005**, *44*, 7520.
16. Zhang, R.; Wang, G.; Guo, S.; Zamora, M. L.; Ying, Q.; Lin, Y.; Wang, W.; Hu, M.; Wang, Y. *Chem. Rev.* **2015**, *115*, 3803.
17. Pöschl, U.; Shiraiwa, M. *Chem. Rev.* **2015**, *115*, 4440.
18. Haywood, J.; Boucher, O. *Rev. Geophys.* **2000**, *38*, 513.
19. Lohmann, U.; Feichter, J. *Atmos. Chem. Phys.* **2005**, *5*, 715.
20. Kulmala, M.; Petäjä, T.; Ehn, M.; Thornton, J.; Sipilä, M.; Worsnop, DR.; Kerminen, V. M. *Annu. Rev. Phys. Chem.* **2014**, *65*, 21.
21. Kolb, C. E.; Jayne, J. T.; Worsnop, D. R.; Molina, M. J.; Meads, R. F.; Viggiano, A. *A. J. Am. Chem. Soc.* **1994**, *116*, 10314.
22. Morokuma, K.; Muguruma, C. *J. Am. Chem. Soc.* **1994**, *116*, 299.
23. Jayne, J. T.; Pöschl, U.; Chen, Y. M.; Dai, D.; Molina, L. T.; Worsnop, D. R.; Kolb, C. E.; Molina, M. J. *J. Phys. Chem. A.* **1997**, *101*, 10000.
24. Torrent-Sucarrat, M.; Francisco, J. S.; Anglada, J. M. *J. Am. Chem. Soc.* **2012**, *134*, 20632.
25. Hazra, M. K.; Sinha, A. *J. Am. Chem. Soc.* **2011**, *133*, 17444.
26. Bandyopadhyay, B.; Kumar, P.; Biswas, P. *J. Phys. Chem. A* **2017**, *121*, 3101.
27. Battye, W. H.; Bray, C. D.; Aneja, V. P.; Tong, D.; Lee, P.; Tang, Y. *Atmos. Environ.* **2017**, *163*, 65.
28. Shen, G.; Suto, M.; Lee, L. C. *J. Geophys. Res.* **1990**, *95*, 13918.
29. Lovejoy, E. R.; Hanson, D. R. *J. Phys. Chem.* **1996**, *100*, 4459.
30. Hirota, K.; Mäkelä, J.; Tokunaga, O. *Ind. Eng. Chem. Res.* **1996**, *35*, 3362.
31. Kim, T. O.; Ishida, T.; Adachi, M.; Okuyama, K.; Seinfeld, J. H. *Aerosol Sci. Technol.* **1998**, *29*, 111.
32. Shi, Z.; Ford, J. V.; Castleman, A. W. *Chem. Phys. Lett.* **1994**, *220*, 274.
33. Kumar, M.; Sinha, A.; Francisco, J. S. *Acc. Chem. Res.* **2016**, *49*, 877.

34. Wong, M. W.; Wiberg, K. B.; Frisch, M. J. *J. Am. Chem. Soc.* **1992**, *114*, 523.
35. And, L. J. L.; Tao, F. M. *J. Phys. Chem. A* **2001**, *105*, 4344.
36. Bork, N.; Elm, J.; Olenius, T.; Vehkamäki, H. *Atmos. Chem. Phys.* **2014**, *14*, 12023.
37. Li, H.; Zhang, X. H.; Zhong, J.; Liu, L.; Zhang, H. J.; Chen, F.; Li, Z. S.; Li, Q. S.; Ge, M. F. *Atmos. Environ.* **2018**, *189*, 244.
38. Sheng, X.; Zhao, H.; Du, L. *Chemosphere.* **2017**, *186*, 331.
39. Elm, J.; Fard, M.; Bilde, M.; and Mikkelsen, V. K. *J. Phys. Chem. A* **2013**, *117*, 12990.
40. Cappa, C. *Nature.* **2016**, *533*, 478.
41. Bianchi, F. ; Trostl, J. ; Junninen, H.; Frege, C.; Henne, S.; Hoyle, CR.; Molteni, U.; Herrmann, E. ; Adamov, A.; Bukowiecki, N.; Chen, X.; Duplissy, J.; Gysel, M.; Hutterli, M.; Kangasluoma, J.; Kontkanen, J.; Kurten, A.; Manninen, HE.; Munch, S. ; Perakyla, O.; Petaja, T.; Rondo, L.; Williamson, C.; Weingartner, E.; Curtius, J.; Worsnop, DR.; Kulmala, M.; Dommen, J.; Baltensperger, U. *Science.* **2016**, *352*, 1109.
42. Molteni, U.; Bianchi, F.; Klein, F.; El Haddad, I.; Frege, C.; Rossi, MJ.; Dommen, J.; Baltensperger, U. *Atmos. Chem. Phys.* **2018**, *18*, 1909.
43. Kurten, A.; Bergen, A.; Heinritzi, M.; Leiminger, M.; Lorenz, V.; Piel, F.; Simon, M.; Sitals, R.; Wagner, AC.; Curtius, J. *Atmos. Chem. Phys.* **2018**, *16*, 12793.
44. Sipila, M.; Sarnela, N.; Jokinen, T.; Henschel, H.; Junninen, H.; Kontkanen, J.; Richters, S.; Kangasluoma, J.; Franchin, A.; Perakyla, O.; Rissanen, MP.; Ehn, M.; Vehkamaki, .H; Kurten, T.; Berndt, T.; Petaja, T.; Worsnop, D.; Ceburnis, D.; Kerminen, VM.; Kulmala, .M; O'Dowd, C. *Nature.* **2016**, *537*, 532.
45. Dawson, M. L.; Varner, M. E.; Perraud, V.; Ezell, MJ.; Gerber, RB.; Finlayson-Pitts, BJ. *P. Natl. Acad. Sci. USA* **2012**, *109*, 18719.
46. Zhang, R.; Molina, M. J. *P. Natl. Acad. Sci. USA.* **2007**, *104*, 5295.
47. Zhang, R.; Wang, L.; Khalizov, A. F.; Zhao, J.; Zheng, J.; Mcgraw, R. L.; Molina, L. T. *P. Natl. Acad. Sci. USA* **2009**, *106*, 17650.
48. Yao, L.; Garmash, O.; Bianchi, F.; Zheng, J.; Yan, C.; Kontkanen, J.; Junninen, H.; Mazon, B. S.; Ehn, M.; Paasonen, P.; Sipilä, M.; Wang, M.; Wang, X.; Xiao, S.; Chen,

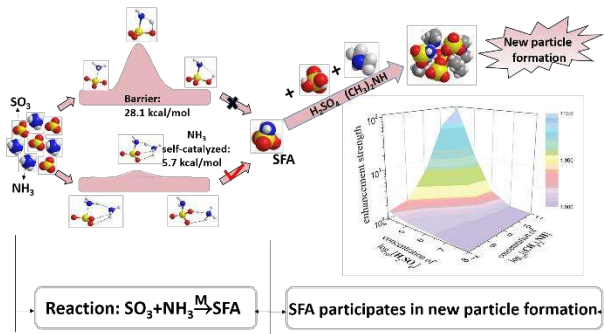
- H.; Lu, Y.; Zhang, B.; Wang, D.; Fu, Q.; Geng, F.; Li, L.; Wang, H.; Qiao, L.; Yang, X.; Chen, J.; Kerminen, V.; Petäjä, T.; Worsnop, D.; Kulmala, M.; Wang, L. *Science*. **2018**, *361*, 278.
49. Guo, S.; Hu, M.; Zamora, M. L.; Peng, J.; Shang, D.; Zheng, J.; Du, Z.; Wu, Z.; Shao, M.; Zeng, L. *P. Natl. Acad. Sci. USA* **2014**, *111*, 17373.
50. Kulmala, M.; Kerminen, V. M.; Petäjä, T.; Ding, A. J.; Wang, L. *Faraday Discuss.* **2017**, *200*, 271.
51. Almeida, J.; Schobesberger, S.; Kürten, A.; Ortega, I. K.; Kupiainenmäättä, O.; Praplan, A. P.; Adamov, A.; Amorim, A.; Bianchi, F.; Breitenlechner, M. *Nature* **2013**, *502*, 359.
52. Riccobono, F.; Schobesberger, S.; Scott, C. E.; Dommen, J.; Ortega, I. K.; Rondo, L.; Almeida, J.; Amorim, A.; Bianchi, F.; Breitenlechner, M. *Science* **2014**, *344*, 717.
53. Kirkby, J.; Duplissy, J.; Sengupta, K.; Frege, C.; Gordon, H.; Williamson, C.; Heinritzi, M.; Simon, M.; Yan, C.; Almeida, J. *Nature* **2016**, *533*, 521.
54. McGrath, M. J.; Olenius, T.; Ortega, I. K.; Loukonen, V.; Paasonen, P.; Kurtén, T.; Kulmala, M.; Ki, H. V. *Atmos. Chem. Phys.* **2011**, *12*, 2345.
55. Frisch, M. J.; Trucks, G. W.; Schlegel, H. B.; Scuseria, G. E.; Robb, M. A.; Cheeseman, J. R.; Scalmani, G.; Barone, V.; Mennucci, B.; Petersson, G. A.; Nakatsuji, H.; Caricato, M.; Li, X.; Hratchian, H. P.; Izmaylov, A. F.; Bloino, J.; Zheng, G.; Sonnenberg, J. L.; Hada, M.; Ehara, M.; Toyota, K.; Fukuda, R.; Hasegawa, J.; Ishida, M.; Nakajima, T.; Honda, Y.; Kitao, O.; Nakai, H.; Vreven, T.; Montgomery, J. A., Jr.; Peralta, J. E.; Ogliaro, F.; Bearpark, M.; Heyd, J. J.; Brothers, E.; Kudin, K. N.; Staroverov, V. N.; Keith, T.; Kobayashi, R.; Normand, J.; Raghavachari, K.; Rendell, A.; Burant, J. C.; Iyengar, S. S.; Tomasi, J.; Cossi, M.; Rega, N.; Millam, J. M.; Klene, M.; Knox, J. E.; Cross, J. B.; Bakken, V.; Adamo, C.; Jaramillo, J.; Gomperts, R.; Stratmann, R. E.; Yazyev, O.; Austin, A. J.; Cammi, R.; Pomelli, C.; Ochterski, J. W.; Martin, R. L.; Morokuma, K.; Zakrzewski, V. G.; Voth, G. A.; Salvador, P.; Dannenberg, J. J.; Dapprich, S.; Daniels, A. D.; Farkas, O.; Foresman, J. B.; Ortiz, J. V.; Cioslowski, J.; Fox, D. J.; *Gaussian 09*, revision A.01; Gaussian Inc.: Wallingford, CT, 2009.
56. Zhao, Y.; Truhlar, D. G. *Theor. Chem. Acc.* **2008**, *120*, 215.
57. Neese, F. *Wires. Comput. Mol. Sci.* **2012**, *2*, 73.
58. Knizia, G.; Adler, T. B.; Werner, H. J. *J. Chem. Phys.* **2009**, *130*, 054104.

59. Peterson, K. A.; Adler, T. B.; Werner, H. J. *J. Chem. Phys.* **2008**, *128*, 084102.
60. Zhang, J.; Dolg, M. *Phys. Chem. Chem. Phys.* **2016**, *18*, 3003.
61. Jorgensen, W. L.; Chandrasekhar, J.; Madura, J. D.; Impey, R. W.; Klein, M. L. *J. Chem. Phys.* **1983**, *79*, 926.
62. Wales, D. J.; Hodges, M. P. *Chem. Phys. Lett.* **1998**, *286*, 65.
63. MacKerell, A. D.; Bashford, D.; Bellott, M.; Dunbrack, RL.; Evanseck, JD.; Field, MJ; Fischer, S; Gao, J; Guo, H; Ha. *J. Phys. Chem. B* **1998**, *102*, 3586.
64. Stewart, J. J. P. *J Comput Aided Mol Des.* **1990**, *4*, 1.
65. Stewart, J. J. P. *Stewart computational chemistry, MOPAC2016, Version: 16. Colorado Springs, CO, USA.*, **2016**.
66. Shampine, L. F.; Reichelt, M. W. *Siam J. Sci. Comput.* **1997**, *18*, 1.
67. Friedlander, S. K. *Physics Today* **1977**, *37*, 1116.
68. Chapman, S.; Cowling, T. G.; Burnett, D. *The Mathematical Theory of Non-uniform Gases*; Burnett, D; Cambridge University Press: Cambridge, **1970**.
69. Lu T, Chen F. *J. Comput. Chem.* **2012**, *33*, 580.
70. Li, H.; Kupiainen-Määttä, O.; Zhang, HJ.; Zhang, XH, Ge, MF. *Atmos. Environ.* **2017**, *166*, 479.
71. Kirkby, J.; Curtius, J.; Almeida, J.; Dunne, E.; Duplissy, J.; Ehrhart, S.; Franchin, A.; Gagne, S.; Ickes, L.; Kuerten, A.; Kupc, A.; Metzger, A.; Riccobono, F.; Rondo, L.; Schobesberger, S.; Tsagkogeorgas, G.; Wimmer, D.; Amorim, A.; Bianchi, F.; Breitenlechner, M.; David, A.; Dommen, J.; Downard, A.; Ehn, M.; Flagan, C. R.; Haider, S.; Hansel, A.; Hauser, D.; Jud, W.; Junninen, H.; Kreissl, F.; Kvashin, A.; Laaksonen, A.; Lehtipalo, K.; Lima, J.; Lovejoy, R. E.; Makhmutov, V.; Mathot, S.; Mikkila, J.; Minginette, P.; Mogo, S.; Nieminen, T.; Onnela, A.; Pereira, P.; Petaja, T.; Schnitzhofer, R.; Seinfeld, H. J.; Sipila, M.; Stozhkov, Y.; Stratmann, F.; Tome, A.; Vanhanen, J.; Viisanen, Y.; Vrtala, A.; Wagner, E. P.; Walther, H.; Weingartner, E.; Wex, H.; Winkler, M. P.; Carslaw, S. K.; Worsnop, R. D.; Baltensperger, U.; Kulmala, M. *Nature*, **2011**, *476*, 429.
72. Olenius, T.; Kupiainen-Määttä, O.; Ortega, I. K.; Kurtén, T.; Vehkamäki. H. *J. Chem. Phys.* **2013**, *139*, 084312.
73. Kulmala, M.; Petaja, T.; Monkkonen, P.; Koponen, IK.; Dal Maso, M.; Aalto, PP.;

- Lehtinen, KEJ.; Kerminen, VM. *Atmos. Chem. Phys.* **2005**, *5*, 409.
74. Gao, J.; Chai, FH.; Wang, T.; Wang, SL.; Wang, WX. *J. Environ. Sci.* **2012**, *24*, 14.
75. Xiao, S.; Wang, MY.; Yao, L.; Kulmala, M.; Zhou, B.; Yang, X.; Chen, JM.; Wang, DF.; Fu, QY.; Worsnop, DR.; Wang, L. *Atmos. Chem. Phys.* **2015**, *15*, 1769.
76. Fliegl, H.; Glöss, A.; Welz, O.; Olzmann, M.; Klopper, W. *J. Chem. Phys.* **2006**, *125*, 54312.
77. Iuga, C.; Alvarez-Idaboy, J. R.; Vivier-Bunge, A. *Theor. Chem. Acc.* **2011**, *129*, 209.
78. Liu, J.; Fang, S.; Wang, Z.; Yi, W.; Tao, F. M.; Liu, J. *Environ. Sci. Technol.* **2015**, *49*, 13112.
79. Tretyakov, MY.; Serov, EA.; Koshelev, MA.; Parshin, VV.; Krupnov, AF. *Phys. Rev. Lett.* **2013**, *110*, 093001.
80. Scribano, Y.; Goldman, N.; Saykally, R. J.; Leforestier, C. *J. Phys. Chem. A.* **2006**, *110*, 5411.
81. Sarangi, C.; Tripathi, S. N.; Mishra, A. K.; Goel, A.; Welton, E. J. *J. Geophys. Res. Atmos.* **2016**, *121*, 7936.
82. Riipinen, I.; Sihto, S. L.; Kulmala, M.; Arnold, F.; Maso, M. D.; Birmili, W.; Saarnio, K.; Teinil, K.; Kerminen, V. M.; Laaksonen, A. *Atmos. Chem. Phys.* **2007**, *7*, 1899.
83. Ge, X.; Wexler, A. S.; Clegg, S. L. *Atmos. Environ.* **2011**, *45*, 524.
84. Kurten, A.; Jokinen, T.; Simon, M.; Sipila, M.; Sarnela, N.; Junninen, H.; Adamov, A.; Almeida, J.; Amorim, A.; Bianchi, F.; Breitenlechner, M.; Dommen, J.; Donahue, NM.; Duplissy, J.; Ehrhart, S.; Flagan, RC.; Franchin, A.; Hakala, J.; Hansel, A.; Heinritzi, M.; Hutterli, M.; Kangasluoma, J.; Kirkby, J.; Laaksonen, A.; Lehtipalo, K.; Leiminger, M.; Makhmutov, V.; Mathot, S.; Onnela, A.; Petaja, T.; Praplan, AP.; Riccobono, F.; Rissanen, MP.; Rondo, L.; Schobesberger, S.; Seinfeld, JH.; Steiner, G.; Tome, A.; Trostl, J.; Winkler, PM.; Williamson, C.; Wimmer, D.; Ye, PL.; Baltensperger, U.; Carslaw, KS.; Kulmala, M.; Worsnop, DR.; Curtius, J. *P. Natl. Acad. Sci.* **2014**, *111*, 15019.
85. Kurten, A.; Li, CX.; Bianchi, F.; Curtius, J.; Dias, A.; Donahue, NM.; Duplissy, J.; Flagan, RC.; Hakala, J.; Jokinen, T.; Kirkby, J.; Kulmala, M.; Laaksonen, A.;

- Lehtipalo, K.; Makhmutov, V.; Onnela, A.; Rissanen, MP.; Simon, M.; Sipila, M.; Stozhkov, Y.; Trostl, J.; Ye, PL.; McMurry, PH. *Atmos. Chem. Phys.* **2018**, *18*, 845.
86. Zhang, HJ.; Kupiainen-Määttä, O.; Zhang, XH.; Molinero, V.; Zhang, YH.; Li, ZS. *J. Chem. Phys.* **2017**, *146*, 184308.
87. Liu, L.; Kupiainen-Määttä, O.; Zhang, HJ.; Li, H.; Zhong, J.; Kurtén, T.; Vehkamäki, H. Zhang, SW.; Zhang, YH.; Ge, MF.; Zhang, XH. Li, ZS. *J. Chem. Phys.* **2018**, *148*, 214303.
88. Liu, L.; Li, Hao.; Zhang, HJ.; Zhong, J.; Bai, Y.; Ge MF.; Li, ZS.; Chen, Y.; Zhang, XH. *Phys. Chem. Chem. Phys.* **2018**, *20*, 17406.

TOC Graphic



Supporting Information

for

Self-Catalytic Reaction of SO₃ and NH₃ to Produce Sulfamic Acid and its Implication to New Particle Formation in the Atmosphere

Hao Li,^{1,2#} Jie Zhong,^{2#} Hanna Vehkamäki,³ Theo Kurtén,⁴ Weigang Wang,⁵ Maofa Ge,⁵ Shaowen Zhang,¹ Zesheng Li,¹ Xiuhui Zhang,^{1*} Joseph S. Francisco,^{2*} Xiao Cheng Zeng^{2,6*}

¹Key Laboratory of Cluster Science, Ministry of Education of China, School of Chemistry and Chemical Engineering, Beijing Institute of Technology, Beijing 100081, P. R. China; ²Department of Chemistry, University of Nebraska-Lincoln, Lincoln, NE, 68588, USA; ³Institute for Atmospheric and Earth System Research/Chemistry, University of Helsinki, PO Box 64 (Gustaf Hällströmin katu 2a), FI-00014, Helsinki, Finland; ⁴Institute for Atmospheric and Earth System Research/Chemistry, University of Helsinki, PO Box 64 (Gustaf Hällströmin katu 2a), FI-00014, Helsinki, Finland; ⁵Beijing National Laboratory for Molecular Sciences (BNLMS), State Key Laboratory for Structural Chemistry of Unstable and Stable Species, Institute of Chemistry, Chinese Academy of Sciences, 100190, Beijing, China; ⁶Beijing Advanced Innovation Center for Soft Matter Science and Engineering, Beijing University of Chemical Technology, Beijing, 100029, China

Authors contribute equally.

Table S1. Gibbs free energies (ΔG) of formation of the clusters containing SFA, SA and DMA, computed at the M06-2X/6-311++G(3df,3pd) level of theory. Energies in kcal mol⁻¹ at three different temperatures (258, 278 and 298 K). SFA, SA and DMA refer to sulfamic acid, sulfuric acid and dimethylamine, respectively.

Table S2. The sum of evaporation rates of the clusters at three different temperatures (258, 278 and 298 K). SFA, SA and DMA refer to sulfamic acid, sulfuric acid and dimethylamine, respectively.

Table S3. The imaginary frequencies (ν , cm⁻¹) of the transition states (TSs) and the Wigner tunneling correction factor (Γ) the reactions of SO₃ and NH₃ without a catalyst, with NH₃ as a self-catalyst and the product SFA as an auto-catalyst at M06-2X/6-311++G(3df,3pd) level of theory.

Table S4. The possible concentration of SFA in the laboratory based on the formation Gibbs free energy at CCSD(T)-F12/cc-pVDZ-F12//M06-2X/6-311++G(3df,3pd) level of theory at 298 K.

Table S5. Possible concentrations of SFA in the atmosphere, based on the formation Gibbs free energy at CCSD(T)-F12/cc-pVDZ-F12//M06-2X/6-311++G(3df,3pd) level of theory, at three different temperatures (298, 288 and 278 K).

Table S6. The ratio ($\frac{r}{r_1}$) of reaction rate for SO₃ + NH₃ reaction self-catalysed by NH₃ and SO₃ + H₂O reaction self-catalysed by H₂O in the conditions of different [NH₃] concentration, and at [(H₂O)₂] = 10¹⁴ molecules cm⁻³.

Table S7. The ratio ($\frac{r}{r_1}$) of reaction rate for SO₃ + NH₃ reaction self-catalysed by NH₃ and SO₃ + H₂O reaction self-catalysed by H₂O in the conditions of different [NH₃] concentration, and at [(H₂O)₂] = 10¹³ molecules cm⁻³.

Table S8. The ratio ($\frac{r}{r_1}$) of reaction rate for SO₃ + NH₃ reaction self-catalysed by NH₃ and SO₃ + H₂O reaction self-catalysed by H₂O in the conditions of different [NH₃] concentration, and at [(H₂O)₂] = 10¹² molecules cm⁻³.

Table S9. The ratio ($\frac{r}{r_1}$) of reaction rate for SO₃ + NH₃ reaction self-catalysed by NH₃ and SO₃ + H₂O reaction self-catalysed by H₂O in the conditions of different [NH₃] concentration, and at [(H₂O)₂] = 10¹¹ molecules cm⁻³.

Table S10. The ratio ($\frac{r}{r_2}$) of reaction rate for SO₃ + NH₃ reaction self-catalysed by NH₃ and SO₃ + H₂O reaction catalysed by NH₃ in the conditions of different [NH₃] concentration, and at [H₂O] = 10¹⁷ molecules cm⁻³.

Table S11. The ratio ($\frac{r}{r_2}$) of reaction rate of $\text{SO}_3 + \text{NH}_3$ reaction self-catalysed by NH_3 to that of SO_3

+ H_2O reaction in different $[\text{NH}_3]$ concentration and at $[\text{H}_2\text{O}] = 10^{16}$ molecules cm^{-3} .

Table S12. The ratio ($\frac{r}{r_2}$) of reaction rate of $\text{SO}_3 + \text{NH}_3$ reaction self-catalysed by NH_3 to that of SO_3

+ H_2O reaction in different $[\text{NH}_3]$ concentration and at $[\text{H}_2\text{O}] = 10^{15}$ molecules cm^{-3} .

Table S13. Formation Gibbs free energies (ΔG) and the sum of evaporation rates of the clusters containing SFA, SA DMA and NH_3 , computed at the M06-2X/6-311++G(3df,3pd) level of theory and 278K. SFA, SA DMA and NH_3 refer to sulfamic acid, sulfuric acid, dimethylamine and ammonia, respectively.

Table S14. Absolute cluster formation rate and enhancement strength of SFA (r_{SFA}) in the conditions of $[\text{SA}] = 10^4 - 10^8$ molecules cm^{-3} , $[\text{DMA}] = 10^7 - 10^{11}$ molecules cm^{-3} , $[\text{SFA}] = 10^4 - 10^8$ molecules cm^{-3} at 298 K. SFA, SA and DMA refer to sulfamic acid, sulfuric acid and dimethylamine, respectively.

Table S15. Absolute cluster formation rate and enhancement strength of SFA (r_{SFA}) in the conditions of $[\text{SA}] = 10^4 - 10^8$ molecules cm^{-3} , $[\text{DMA}] = 10^7 - 10^{11}$ molecules cm^{-3} , $[\text{SFA}] = 10^4 - 10^8$ molecules cm^{-3} at 278 K. SFA, SA and DMA refer to sulfamic acid, sulfuric acid and dimethylamine, respectively.

Table S16. Absolute cluster formation rate and enhancement strength of SFA (r_{SFA}) in the conditions of $[\text{SA}] = 10^4 - 10^8$ molecules cm^{-3} , $[\text{DMA}] = 10^7 - 10^{11}$ molecules cm^{-3} , $[\text{SFA}] = 10^4 - 10^8$ molecules cm^{-3} at 258 K. SFA, SA and DMA refer to sulfamic acid, sulfuric acid and dimethylamine, respectively.

Figure S1. (a) The ratio of cluster formation rates (r_{SFA}) versus the logarithm of $[\text{SA}]$; at $[\text{DMA}] = 10^9$ molecules cm^{-3} , and (b) the ratio of cluster formation rates (r_{SFA}) versus the logarithm of $[\text{DMA}]$, at $T = 298$ K and $[\text{SFA}] = 10^4-10^8$ molecules cm^{-3} . SFA, SA and DMA refer to sulfamic acid, sulfuric acid and dimethylamine, respectively.

Figure S2. (a) The ratio of cluster formation rates (r_{SFA}) versus the logarithm of $[\text{SA}]$; at $[\text{DMA}] = 10^9$ molecules cm^{-3} , and (b) the ratio of cluster formation rates (r_{SFA}) versus the logarithm of $[\text{DMA}]$, at $T = 258$ K and $[\text{SFA}] = 10^4-10^8$ molecules cm^{-3} . SFA, SA and DMA refer to sulfamic acid, sulfuric acid and dimethylamine, respectively.

Figure S3. (a) The ratio (r) of cluster formation rates versus the logarithm of $[\text{DMA}]$ at $[\text{SA}] = 10^6$ molecules cm^{-3} , $[\text{NH}_3] = 10^{10}$ molecules cm^{-3} , $[\text{SFA}] = 10^4-10^7$ molecules cm^{-3} and $T = 278$ K. (b) The ratio (r) of cluster formation rates versus the logarithm of $[\text{DMA}]$ at $[\text{SA}] = 10^6$ molecules cm^{-3} , $[\text{NH}_3] = 10^{11}$ molecules cm^{-3} , $[\text{SFA}] = 10^4-10^7$ molecules cm^{-3} and $T = 278$ K. SFA, SA, DMA and NH_3 refer to sulfamic acid, sulfuric acid, dimethylamine and ammonia, respectively.

Table S1. Gibbs free energies (ΔG) of formation of the clusters containing SFA, SA and DMA, computed at the M06-2X/6-311++G(3df,3pd) level of theory. Energies in kcal mol⁻¹ at three different temperatures (258, 278 and 298 K). SFA, SA and DMA refer to sulfamic acid, sulfuric acid and dimethylamine, respectively.

Clusters	$\Delta G_{258K}(\text{kcal/mol})$	$\Delta G_{278K}(\text{kcal/mol})$	$\Delta G_{298K}(\text{kcal/mol})$
SA·DMA	-12.53	-11.85	-11.16
SFA·DMA	-9.02	-8.25	-7.48
(SA) ₂	-9.77	-9.10	-8.42
(SFA) ₂	-9.33	-8.50	-7.68
SFA·SA	-10.54	-9.72	-8.90
(SA) ₂ ·DMA	-33.26	-31.71	-30.15
SFA·SA·DMA	-31.93	-30.37	-28.81
(SFA) ₂ ·DMA	-27.96	-27.96	-24.81
(SA) ₃	-17.00	-15.46	-14.16
(SFA) ₃	-17.60	-15.93	-14.26
SFA·(SA) ₂	-19.53	-17.90	-16.25
(SFA) ₂ ·SA	-17.46	-15.88	-14.27
(SA) ₂ ·(DMA) ₂	-49.56	-47.24	-44.92
SFA·SA·(DMA) ₂	-46.84	-44.47	-42.08
(SFA) ₂ ·(DMA) ₂	-41.18	-39.05	-36.90
(SA) ₃ ·DMA	-46.84	-44.46	-42.07
SFA·(SA) ₂ ·DMA	-45.73	-43.28	-40.81
(SFA) ₂ ·SA·DMA	-42.74	-42.74	-37.87
(SFA) ₃ ·DMA	-39.06	-36.67	-34.28
(SA) ₃ ·(DMA) ₂	-66.28	-63.15	-60.37
SFA·(SA) ₂ ·(DMA) ₂	-63.20	-59.98	-56.75
(SFA) ₂ ·SA·(DMA) ₂	-60.71	-57.46	-54.19
(SFA) ₃ ·(DMA) ₂	-53.73	-50.34	-46.94

Table S2. The sum of evaporation rates of the clusters at three different temperatures (258, 278 and 298 K). SFA, SA and DMA refer to sulfamic acid, sulfuric acid and dimethylamine, respectively.

Clusters	The sum of evaporation rates (s^{-1})		
	258 K	278 K	298 K
SA·DMA	3.26×10^{-2}	6.25	8.24×10^1
SFA·DMA	3.23×10^2	4.44×10^3	4.32×10^4
(SA) ₂	7.39×10^1	3.14×10^2	2.91×10^3
(SFA) ₂	1.94×10^2	1.04×10^3	1.13×10^4
SFA·SA	1.16×10^1	2.16×10^2	2.74×10^3
(SA) ₂ ·DMA	4.04×10^{-8}	3.45×10^{-6}	1.65×10^{-4}
SFA·SA·DMA	5.78×10^{-7}	4.17×10^{-5}	1.69×10^{-3}
(SFA) ₂ ·DMA	5.02×10^{-6}	2.63×10^{-4}	8.45×10^{-3}
(SA) ₃	1.05×10^4	1.34×10^5	8.03×10^5
(SFA) ₃	1.57×10^3	2.21×10^4	2.22×10^5
SFA·(SA) ₂	4.42×10^2	7.05×10^3	8.17×10^4
(SFA) ₂ ·SA	2.35×10^4	2.39×10^5	1.86×10^6
(SA) ₂ ·(DMA) ₂	3.33×10^{-4}	1.27×10^{-2}	2.97×10^{-1}
SFA·SA·(DMA) ₂	5.06×10^{-3}	1.71×10^{-1}	3.76
(SFA) ₂ ·(DMA) ₂	1.40×10^{-1}	2.38	2.82×10^1
(SA) ₃ ·DMA	4.48×10^{-2}	1.30	2.43×10^1
SFA·(SA) ₂ ·DMA	4.37×10^{-1}	1.25	2.34×10^2
(SFA) ₂ ·SA·DMA	1.05×10^1	2.22×10^2	3.20×10^3
(SFA) ₃ ·DMA	6.10	1.23×10^2	1.64×10^3
(SA) ₃ ·(DMA) ₂	1.15×10^{-4}	5.04×10^{-3}	7.42×10^{-2}
SFA·(SA) ₂ ·(DMA) ₂	4.87×10^{-2}	1.63	3.47×10^1
(SFA) ₂ ·SA·(DMA) ₂	3.08×10^{-2}	1.02	2.13×10^1
(SFA) ₃ ·(DMA) ₂	4.54×10^{-1}	2.48×10^1	7.86×10^2

As equation (6) shows, the evaporation coefficient depends exponentially on formation free energies, which means that small differences in free energies can lead to large differences in evaporation coefficient, and thus the accuracy of these calculations is very important. The discrepancies of the evaporation rates are attributed to the different computation method used. In the present paper, M06-2X functional is chosen to calculate the cluster formation free energies. For SA·DMA cluster, the formation free energy computed based on M06-2X is 4.24 kcal/mol less negative than that based on the B3RICC2 method¹, resulting in a difference of evaporation rates more than 3 orders of magnitude. Many recent benchmark studies²⁻⁸ for the performance of different theoretical methods on hydrogen-bonded clusters indicate that the B3RICC2 method may overestimate the free energies of sulfuric acid-base clusters and thus underestimate their evaporation rates. The M06-2X method²⁻¹¹ has been found to be reasonably close to coupled-cluster values (a fairly high-level calculation) and has been shown to be one of the most reliable and accurate density functional theory methods with respect to free energies of molecular clusters, and thus evaporation rates. Thus, the evaporation rates obtained from M06-2X functional appears to be more reliable.

The tunneling correction

Table S3. The computed imaginary frequencies (ν , cm⁻¹) of the transition states (TSs) and the Wigner tunneling correction factor (Γ) the reactions of SO₃ and NH₃ without a catalyst, with NH₃ being as a self-catalyst and the product SFA as an auto-catalyst at M06-2X/6-311++G(3df,3pd) level of theory.

	Without a catalyst	Self-catalyst	Auto-catalyst
ν	1686 cm ⁻¹	646 cm ⁻¹	837 cm ⁻¹
Γ	3.77	1.41	1.68

The tunneling effects could affect the reaction rate involving hydrogen atom transfer. Thus, we further examine the effect of tunneling correction and the corresponding reaction rate constant through the Wigner tunneling correction by a factor Γ as

$$\Gamma = 1 + \frac{1}{24} \left(\frac{hv^{\mp}}{k_B T} \right)^2 \quad (\text{S1})$$

where h is the Planck's constant, k_B is the Boltzmann's constant, T is the temperature, and v^{\mp} is the imaginary frequency of the transition state. The data of Γ for all hydration reactions in the present study are listed in Table S3. The result shows that the maximum value of the Γ among all the reactions considered in the present study is 3.77 (the uncatalysed hydration reaction), suggesting that the tunneling effect has

little influence on the reaction rate constant.

The concentration of sulfamic acid ($\text{H}_2\text{NSO}_3\text{H}$, SFA)

To the best of our knowledge, the concentration of SFA has not been determined. Here, the equilibrium concentration of SFA can be roughly estimated theoretically using the following expression: $[\text{SFA}] = K_{\text{SO}_3-\text{NH}_3}[\text{SO}_3][\text{NH}_3]$, where $K_{\text{SO}_3-\text{NH}_3}$ is equal to the equilibrium constant from the formation Gibbs energy of the SFA. $[\text{SO}_3]$ and $[\text{NH}_3]$ are the concentration of SO_3 and NH_3 monomer, respectively. To explain the observed spectral signal and measured experimental reaction rate constant, we use the reactant concentrations of $[\text{SO}_3] = 10^9\text{-}10^{13}$ molecules cm^{-3} , $[\text{NH}_3] = 10^{13}$ molecules cm^{-3} with the same values as laboratory measurements. According to the above equation, the estimated concentration of the reaction product, SFA, is about $10^{11}\text{-}10^{15}$ molecules cm^{-3} as shown in **Table S4**. Meanwhile, considering the rapid reaction rate constant and the relatively closed environment in the experiment, the reaction product could be collected in a short time. On the other hand, in realistic atmosphere (**Table S5**), there exist some other possible sinks for this product, such as nucleation and condensation. In this case, the concentration of SO_3 is much lower than 10^{11} molecules cm^{-3} . In normal atmospheric conditions, the main source of SO_3 is the oxidation of SO_2 and its major loss is the reaction with water to form sulfuric acid as the following equations:



Here, possible third bodies and/or catalysts are not considered. Due to higher barrier for the reaction (S3) than that of reaction (S2), and the much higher concentration of O_2 than OH , the first step is rate-limiting, i.e. the formation rate of SO_3 depends on $[\text{SO}_2][\text{OH}]$. Thus, we can estimate SO_3 concentration using the pseudo-steady-state approach:

$$\frac{d[\text{SO}_3]}{dt} = k_{\text{S1}}[\text{SO}_2][\text{OH}] - k_{\text{S3}}[\text{SO}_3][\text{H}_2\text{O}] = 0 \quad (\text{S5})$$

$$[\text{SO}_3] = k_{\text{S1}}[\text{SO}_2][\text{OH}] / k_{\text{S3}}[\text{H}_2\text{O}] \quad (\text{S6})$$

where k_{S2} and k_{S4} denote the reaction rate coefficients for reaction (S2) and reaction (S4), respectively. The effective bimolecular reaction rate coefficients (at 298 K and 1 atm) are taken as follows: k_{S2} is taken to be 1.3×10^{-12} cm^3 molecule $^{-1}$ s^{-1} and k_{S4} is taken to be 2.4×10^{-15} cm^3 molecule $^{-1}$ s^{-1} .¹² The tropospheric SO_2 concentration typically varies between 20 and 1500 ppt from marine boundary-layer air to polluted

continental air,¹³ corresponding to a range from 10^9 to 10^{11} molecules cm^{-3} . The atmospheric concentration of H_2O varies between about 10^{15} and 10^{17} molecules cm^{-3} . The OH concentration is typically around 10^6 molecules cm^{-3} .¹⁴ Using these values and ranges for $k_{\text{S}2}$, $k_{\text{S}4}$ and the three concentrations mentioned above, we obtain a range of 1 to 10^5 molecules cm^{-3} for SO_3 . Thus, in the atmospheric conditions, a wide range concentration of SFA, from 10^4 to 10^8 molecules cm^{-3} , is selected.

Table S4. The possible concentration of SFA in the laboratory based on the formation Gibbs free energy at CCSD(T)-F12/cc-pVDZ-F12//M06-2X/6-311++G(3df,3pd) level of theory at 298 K.

Product	ΔG (kcal/ mol)	[SO_3] (molecules cm^{-3})	[NH_3] (molecules cm^{-3})	[SFA] (molecules cm^{-3})	Possible [SFA] in laboratory conditions (molecules cm^{-3})
SFA	-10.83	$10^9 - 10^{13}$	10^{13}	3.52×10^{14}	$10^{11} - 10^{15}$

Table S5. Possible concentrations of SFA in the atmosphere, based on the formation Gibbs free energy at CCSD(T)-F12/cc-pVDZ-F12//M06-2X/6-311++G(3df,3pd) level of theory, at three different temperatures (298, 288 and 278 K).

Product	ΔG (kcal/mol)	[SO_3] (molecules cm^{-3})	[NH_3] (molecules cm^{-3})	[SFA] (molecules cm^{-3})	Possible [SFA] in atmospheric conditions (molecules cm^{-3})
SFA	-10.61 at 298 K			2.43×10^6	
	-10.98 at 288 K	$10^0 - 10^5$	10^{13}	8.33×10^6	$10^4 - 10^8$
	-11.34 at 278 K			3.08×10^7	

Competition reactions between SO₃ with NH₃ and SO₃ with H₂O

The reaction rate for SO₃ + NH₃ reaction catalysed by M (M = NH₃) can be expressed as equation (S7) (also listed in the manuscript):

$$r = k[\text{SO}_3][\text{NH}_3][\text{M}] \quad (\text{S7})$$

For SO₃ + H₂O reaction, the reaction rate with a second water or an ammonia (NH₃) molecule as a catalyst can be expressed by equations (S8) and (S9) as follows:

$$r_1 = k_1[\text{SO}_3][(H_2O)_2] \quad (\text{S8})$$

$$r_2 = k_2[\text{SO}_3][\text{NH}_3 - \text{H}_2\text{O}] \quad (\text{S9})$$

where k_1 (10^{-11} cm³ molecule⁻¹ s⁻¹)¹⁵ or k_2 (10^{-5} cm³ molecule⁻¹ s⁻¹)¹⁶ is the reaction rate constant for SO₃ and H₂O reaction catalysed by H₂O or NH₃ molecule. [SO₃], [(H₂O)₂] and [NH₃-H₂O] stand for the concentration of SO₃, (H₂O)₂ and NH₃-H₂O dimer, respectively.

The ratio of reaction rate for SO₃ + NH₃ reaction to that for SO₃ + H₂O reaction is given as follows:

$$\frac{r}{r_1} = \frac{k * [\text{SO}_3][\text{NH}_3]}{k_1 * [\text{SO}_3][(H_2O)_2]} = \frac{k * [\text{NH}_3]}{k_1 * [(H_2O)_2]} \quad (\text{S10})$$

$$\frac{r}{r_2} = \frac{k * [\text{SO}_3][\text{NH}_3]}{k_2 * [\text{SO}_3][\text{NH}_3 - \text{H}_2\text{O}]} = \frac{k * [\text{NH}_3]}{k_2 * [\text{NH}_3 - \text{H}_2\text{O}]} \quad (\text{S11})$$

According to the above calculation, the ratios of $\frac{r}{r_1}$ and $\frac{r}{r_2}$ in the conditions of

different reactant concentration are shown in Tables S6-S12. The ratios from 10^{-1} to 1 are written in red. The results indicate that the reaction of SO₃ and NH₃ has the possibility to be competitive with the reaction of SO₃ and H₂O, especially at high [NH₃] and low [H₂O] concentration.

Table S6. The ratio ($\frac{r}{r_1}$) of reaction rate for $\text{SO}_3 + \text{NH}_3$ reaction self-catalysed by

NH_3 and $\text{SO}_3 + \text{H}_2\text{O}$ reaction self-catalysed by H_2O in the conditions of different $[\text{NH}_3]$ concentration, and at $[(\text{H}_2\text{O})_2] = 10^{14}$ molecules cm^{-3} .

$[\text{NH}_3]$ (molecules cm^{-3})	$\frac{r}{r_1}$
10^{13}	$2.72*10^{-1}$
10^{12}	$1.45*10^{-2}$
10^{11}	$2.55*10^{-4}$
10^{10}	$2.76*10^{-6}$
10^9	$2.78*10^{-8}$

Table S7. The ratio ($\frac{r}{r_1}$) of reaction rate for $\text{SO}_3 + \text{NH}_3$ reaction self-catalysed by

NH_3 and $\text{SO}_3 + \text{H}_2\text{O}$ reaction self-catalysed by H_2O in the conditions of different $[\text{NH}_3]$ concentration, and at $[(\text{H}_2\text{O})_2] = 10^{13}$ molecules cm^{-3} .

$[\text{NH}_3]$ (molecules cm^{-3})	$\frac{r}{r_1}$
10^{13}	2.72
10^{12}	$1.45*10^{-1}$
10^{11}	$2.55*10^{-3}$
10^{10}	$2.76*10^{-5}$
10^9	$2.78*10^{-7}$

Table S8. The ratio ($\frac{r}{r_1}$) of reaction rate for $\text{SO}_3 + \text{NH}_3$ reaction self-catalysed by

NH_3 and $\text{SO}_3 + \text{H}_2\text{O}$ reaction self-catalysed by H_2O in the conditions of different $[\text{NH}_3]$ concentration, and at $[(\text{H}_2\text{O})_2] = 10^{12}$ molecules cm^{-3} .

$[\text{NH}_3]$ (molecules cm^{-3})	$\frac{r}{r_1}$
10^{13}	$2.72*10^1$
10^{12}	1.45
10^{11}	$2.55*10^{-2}$
10^{10}	$2.76*10^{-4}$
10^9	$2.78*10^{-6}$

Table S9. The ratio ($\frac{r}{r_1}$) of reaction rate for $\text{SO}_3 + \text{NH}_3$ reaction self-catalysed by

NH_3 and $\text{SO}_3 + \text{H}_2\text{O}$ reaction self-catalysed by H_2O , in the conditions of different $[\text{NH}_3]$ concentration, and at $[(\text{H}_2\text{O})_2] = 10^{11}$ molecules cm^{-3} .

$[\text{NH}_3]$ (molecules cm^{-3})	$\frac{r}{r_1}$
10^{13}	$2.72*10^2$
10^{12}	$1.45*10^1$
10^{11}	$2.55*10^{-1}$
10^{10}	$2.76*10^{-3}$
10^9	$2.78*10^{-5}$

Table S10. The ratio ($\frac{r}{r_2}$) of reaction rate for $\text{SO}_3 + \text{NH}_3$ reaction self-catalysed by

NH_3 and $\text{SO}_3 + \text{H}_2\text{O}$ reaction catalysed by NH_3 in the conditions of different $[\text{NH}_3]$ concentration, and at $[\text{H}_2\text{O}] = 10^{17}$ molecules cm^{-3} .

$[\text{NH}_3]$ (molecules cm^{-3})	$\frac{r}{r_2}$
10^{13}	$2.72*10^{-2}$
10^{12}	$1.45*10^{-2}$
10^{11}	$2.55*10^{-3}$
10^{10}	$2.76*10^{-4}$
10^9	$2.72*10^{-5}$

Table S11. The ratio ($\frac{r}{r_2}$) of reaction rate for $\text{SO}_3 + \text{NH}_3$ reaction self-catalysed by

NH_3 and $\text{SO}_3 + \text{H}_2\text{O}$ reaction catalysed by NH_3 in the conditions of different $[\text{NH}_3]$ concentration, and at $[\text{H}_2\text{O}] = 10^{16}$ molecules cm^{-3} .

$[\text{NH}_3]$ (molecules cm^{-3})	$\frac{r}{r_2}$
10^{13}	$2.72*10^{-1}$
10^{12}	$1.45*10^{-1}$
10^{11}	$2.55*10^{-2}$
10^{10}	$2.76*10^{-3}$
10^9	$2.72*10^{-4}$

Table S12. The ratio ($\frac{r}{r_2}$) of reaction rate of $\text{SO}_3 + \text{NH}_3$ reaction self-catalysed by NH_3 to that of $\text{SO}_3 + \text{H}_2\text{O}$ reaction in different $[\text{NH}_3]$ concentration and at $[\text{H}_2\text{O}] = 10^{15}$ molecules cm^{-3} .

$[\text{NH}_3]$ (molecules cm^{-3})	$\frac{r}{r_2}$
10^{13}	2.72
10^{12}	1.45
10^{11}	2.55*10 ⁻¹
10^{10}	2.76*10 ⁻²
10^9	2.72*10 ⁻³

Table S13. Formation Gibbs free energies (ΔG) and the sum of evaporation rates of the clusters containing SFA, SA DMA and NH_3 , computed at the M06-2X/6-311++G(3df,3pd) level of theory and 278 K. SFA, SA DMA and NH_3 refer to sulfamic acid, sulfuric acid, dimethylamine and ammonia, respectively.

Clusters	$\Delta G_{278\text{K}}$ (kcal/mol)	The sum of evaporation rates (s^{-1})
$\text{SA}\cdot\text{NH}_3$	-9.45	4.36*10 ²
$\text{SFA}\cdot\text{NH}_3$	-5.69	4.19*10 ⁵
$(\text{SA})_2\cdot\text{NH}_3$	-23.92	9.98*10 ⁻²
$\text{SFA}\cdot\text{SA}\cdot\text{NH}_3$	-22.76	1.74
$(\text{SFA})_2\cdot\text{NH}_3$	-18.99	1.34*10 ²
$(\text{SA})_2\cdot(\text{NH}_3)_2$	-31.83	1.35*10 ⁴
$\text{SFA}\cdot\text{SA}\cdot(\text{NH}_3)_2$	-30.07	4.24*10 ⁴
$(\text{SFA})_2\cdot(\text{NH}_3)_2$	-27.37	6.10*10 ³
$(\text{SA})_2\cdot\text{DMA}\cdot\text{NH}_3$	-39.44	1.88*10 ⁴
$(\text{SFA})_2\cdot\text{DMA}\cdot\text{NH}_3$	-32.60	3.07*10 ⁵
$\text{SA}\cdot(\text{DMA})_2\cdot\text{NH}_3$	-43.29	1.45
$\text{SA}\cdot\text{SFA}\cdot\text{DMA}\cdot\text{NH}_3$	-36.85	1.83*10 ⁵

Table S14. Absolute cluster formation rate and enhancement strength of SFA (r_{SFA}) in the conditions of $[\text{SA}] = 10^4 - 10^8$ molecules cm^{-3} , $[\text{DMA}] = 10^7 - 10^{11}$ molecules cm^{-3} , $[\text{SFA}] = 10^4 - 10^8$ molecules cm^{-3} at 298 K. SFA, SA and DMA refer to sulfmaic acid, sulfuric acid and dimethylamine, respectively.

[SA] (molecules cm^{-3})	[DMA] (molecules cm^{-3})	[SFA] (molecules cm^{-3})	Absolute cluster formation rate	Enhancement strength (r_{SFA})
10^4	10^7	10^4	2.27×10^{-9}	1.01
10^5	10^7	10^4	2.26×10^{-6}	1.00
10^6	10^7	10^4	2.30×10^{-3}	1.00
10^7	10^7	10^4	2.37	1.00
10^8	10^7	10^4	8.41×10^2	1.00
10^4	10^8	10^4	3.22×10^{-7}	1.03
10^5	10^8	10^4	3.08×10^{-4}	1.01
10^6	10^8	10^4	2.47×10^{-1}	1.00
10^7	10^8	10^4	8.29×10^1	1.00
10^8	10^8	10^4	1.08×10^4	1.00
10^4	10^9	10^4	8.15×10^{-6}	1.22
10^5	10^9	10^4	6.50×10^{-3}	1.02
10^5	10^9	10^4	4.28	1.00
10^7	10^9	10^4	9.80×10^2	1.00
10^8	10^9	10^4	1.12×10^5	1.00
10^4	10^{10}	10^4	2.10×10^{-4}	2.08
10^5	10^{10}	10^4	1.05×10^{-1}	1.11
10^6	10^{10}	10^4	5.81×10^1	1.01
10^7	10^{10}	10^4	1.11×10^4	1.00
10^8	10^{10}	10^4	1.20×10^6	1.00
10^4	10^{11}	10^4	1.04×10^{-2}	1.68
10^5	10^{11}	10^4	5.58	1.07
10^6	10^{11}	10^4	1.85×10^3	1.01
10^7	10^{11}	10^4	2.36×10^5	1.00
10^8	10^{11}	10^4	2.38×10^7	1.00
10^4	10^7	10^5	2.46×10^{-9}	1.10
10^5	10^7	10^5	2.34×10^{-6}	1.04
10^6	10^7	10^5	2.40×10^{-3}	1.04
10^7	10^7	10^5	2.39	1.01
10^8	10^7	10^5	8.41×10^2	1.00
10^4	10^8	10^5	3.99×10^{-7}	1.27
10^5	10^8	10^5	3.25×10^{-4}	1.06
10^6	10^8	10^5	2.54×10^{-1}	1.03
10^7	10^8	10^5	8.35×10^1	1.01
10^8	10^8	10^5	1.08×10^4	1.00
10^4	10^9	10^5	2.18×10^{-5}	3.26
10^5	10^9	10^5	8.00×10^{-3}	1.25

10^6	10^9	10^5	4.46	1.05
10^7	10^9	10^5	9.88×10^2	1.01
10^8	10^9	10^5	1.12×10^5	1.00
10^4	10^{10}	10^5	1.20×10^3	1.19
10^5	10^{10}	10^5	1.97×10^{-1}	2.07
10^6	10^{10}	10^5	6.33×10^1	1.10
10^7	10^{10}	10^5	1.11×10^4	1.01
10^8	10^{10}	10^5	1.21×10^6	1.00
10^4	10^{11}	10^5	4.85×10^{-2}	7.82
10^5	10^{11}	10^5	8.61	1.64
10^6	10^{11}	10^5	1.93×10^3	1.05
10^7	10^{11}	10^5	2.37×10^5	1.00
10^8	10^{11}	10^5	2.38×10^7	1.00
10^4	10^7	10^6	4.78×10^{-9}	2.13
10^5	10^7	10^6	3.20×10^{-6}	1.42
10^6	10^7	10^6	2.90×10^{-3}	1.26
10^7	10^7	10^6	2.56	1.08
10^8	10^7	10^6	8.49×10^2	1.01
10^4	10^8	10^6	1.38×10^{-6}	4.39
10^5	10^8	10^6	5.13×10^{-4}	1.67
10^6	10^8	10^6	3.23×10^{-1}	1.31
10^7	10^8	10^6	8.98×10^1	1.08
10^8	10^8	10^6	1.09×10^4	1.01
10^4	10^9	10^6	1.90×10^{-4}	2.84×10^1
10^5	10^9	10^6	2.57×10^{-2}	4.02
10^6	10^9	10^6	6.45	1.51
10^7	10^9	10^6	1.07×10^3	1.09
10^8	10^9	10^6	1.13×10^5	1.01
10^4	10^{10}	10^6	1.10×10^{-2}	1.09×10^2
10^5	10^{10}	10^6	1.11	1.17×10^1
10^6	10^{10}	10^6	1.15×10^2	2.00
10^7	10^{10}	10^6	1.21×10^4	1.09
10^8	10^{10}	10^6	1.22×10^6	1.01
10^4	10^{11}	10^6	4.29×10^{-1}	6.93×10^1
10^5	10^{11}	10^6	3.76×10^1	7.18
10^6	10^{11}	10^6	2.75×10^3	1.49
10^7	10^{11}	10^6	2.46×10^5	1.05
10^8	10^{11}	10^6	2.39×10^7	1.00
10^4	10^7	10^7	5.37×10^{-8}	2.39×10^1
10^5	10^7	10^7	1.26×10^{-5}	5.59
10^6	10^7	10^7	7.60×10^{-3}	3.30
10^7	10^7	10^7	4.16	1.75
10^8	10^7	10^7	9.24×10^2	1.10
10^4	10^8	10^7	2.80×10^{-5}	8.90×10^1

10^5	10^8	10^7	3.80×10^{-3}	1.24×10^1
10^6	10^8	10^7	1.04	4.23
10^7	10^8	10^7	1.52×10^2	1.84
10^8	10^8	10^7	1.19×10^4	1.10
10^4	10^9	10^7	3.80×10^{-3}	5.69×10^2
10^5	10^9	10^7	3.71×10^{-1}	5.80×10^1
10^5	10^9	10^7	3.24×10^1	7.61
10^7	10^9	10^7	1.85×10^3	1.89
10^8	10^9	10^7	1.23×10^5	1.10
10^4	10^{10}	10^7	1.50×10^{-1}	1.48×10^3
10^5	10^{10}	10^7	1.27×10^1	1.34×10^2
10^6	10^{10}	10^7	6.21×10^2	1.08×10^1
10^7	10^{10}	10^7	2.09×10^4	1.90
10^8	10^{10}	10^7	1.31×10^6	1.09
10^4	10^{11}	10^7	8.35	1.35×10^3
10^5	10^{11}	10^7	3.89×10^2	7.42×10^1
10^6	10^{11}	10^7	9.99×10^3	5.43
10^7	10^{11}	10^7	3.40×10^5	1.44
10^8	10^{11}	10^7	2.49×10^7	1.04
10^4	10^7	10^8	1.19×10^{-6}	5.30×10^2
10^5	10^7	10^8	1.38×10^{-4}	6.13×10^1
10^6	10^7	10^8	3.23×10^{-2}	1.40×10^1
10^7	10^7	10^8	1.54×10^1	6.48
10^8	10^7	10^8	1.65×10^3	1.96
10^4	10^8	10^8	8.66×10^{-4}	2.76×10^3
10^5	10^8	10^8	8.85	2.89×10^2
10^6	10^8	10^8	9.98	4.05×10^1
10^7	10^8	10^8	7.39×10^2	8.92
10^8	10^8	10^8	2.16×10^4	2.00
10^4	10^9	10^8	1.02×10^{-1}	1.52×10^4
10^5	10^9	10^8	8.87	1.39×10^3
10^6	10^9	10^8	4.37×10^2	1.03×10^2
10^7	10^9	10^8	9.74×10^3	9.95
10^8	10^9	10^8	2.21×10^5	1.97
10^4	10^{10}	10^8	6.69	6.61×10^4
10^5	10^{10}	10^8	3.04×10^2	3.20×10^3
10^6	10^{10}	10^8	6.21×10^3	1.08×10^2
10^7	10^{10}	10^8	9.95×10^4	9.01
10^8	10^{10}	10^8	2.25×10^6	1.87
10^4	10^{11}	10^8	3.06×10^2	4.94×10^4
10^5	10^{11}	10^8	5.71×10^3	1.09×10^3
10^6	10^{11}	10^8	7.57×10^4	4.11×10^1
10^7	10^{11}	10^8	1.16×10^6	4.91
10^8	10^{11}	10^8	3.42×10^7	1.43

Table S15. Absolute cluster formation rate and enhancement strength of SFA (r_{SFA}) in the conditions of $[\text{SA}] = 10^4 - 10^8$ molecules cm^{-3} , $[\text{DMA}] = 10^7 - 10^{11}$ molecules cm^{-3} , $[\text{SFA}] = 10^4 - 10^8$ molecules cm^{-3} at 278 K. SFA, SA and DMA refer to sulfmaic acid, sulfuric acid and dimethylamine, respectively.

[SA] (molecules cm^{-3})	[DMA] (molecules cm^{-3})	[SFA] (molecules cm^{-3})	Absolute cluster formation rate	Enhancement strength (r_{SFA})
10^4	10^7	10^4	1.09×10^{-10}	1.06
10^5	10^7	10^4	1.04×10^{-7}	1.01
10^6	10^7	10^4	1.08×10^{-4}	1.00
10^7	10^7	10^4	1.41×10^{-1}	1.00
10^8	10^7	10^4	1.86×10^2	1.00
10^4	10^8	10^4	2.34×10^{-8}	1.15
10^5	10^8	10^4	2.07×10^{-5}	1.02
10^6	10^8	10^4	2.02×10^{-2}	1.00
10^7	10^8	10^4	1.87×10^1	1.00
10^8	10^8	10^4	1.11×10^4	1.00
10^4	10^9	10^4	9.75×10^{-7}	1.81
10^5	10^9	10^4	5.80×10^{-4}	1.08
10^5	10^9	10^4	5.35×10^{-1}	1.01
10^7	10^9	10^4	4.76×10^2	1.00
10^8	10^9	10^4	2.29×10^5	1.00
10^4	10^{10}	10^4	3.24×10^{-5}	2.10
10^5	10^{10}	10^4	1.70×10^{-2}	1.10
10^6	10^{10}	10^4	1.52×10^1	1.01
10^7	10^{10}	10^4	1.26×10^4	1.00
10^8	10^{10}	10^4	4.20×10^6	1.00
10^4	10^{11}	10^4	4.40×10^{-3}	1.26
10^5	10^{11}	10^4	3.53	1.03
10^6	10^{11}	10^4	3.13×10^3	1.00
10^7	10^{11}	10^4	1.43×10^6	1.00
10^8	10^{11}	10^4	1.76×10^8	1.00
10^4	10^7	10^5	1.60×10^{-10}	1.55
10^5	10^7	10^5	1.09×10^{-7}	1.06
10^6	10^7	10^5	1.08×10^{-4}	1.01
10^7	10^7	10^5	1.41×10^{-1}	1.00
10^8	10^7	10^5	1.86×10^2	1.00
10^4	10^8	10^5	5.11×10^{-8}	2.51
10^5	10^8	10^5	2.34×10^{-5}	1.15
10^6	10^8	10^5	2.05×10^{-2}	1.01
10^7	10^8	10^5	1.88×10^1	1.00
10^8	10^8	10^5	1.11×10^4	1.00
10^4	10^9	10^5	4.91×10^{-6}	9.14
10^5	10^9	10^5	9.74×10^{-4}	1.81

10^6	10^9	10^5	5.74×10^{-1}	1.08
10^7	10^9	10^5	4.80×10^2	1.01
10^8	10^9	10^5	2.29×10^5	1.00
10^4	10^{10}	10^5	1.85×10^4	1.20×10^1
10^5	10^{10}	10^5	3.23×10^{-2}	2.10
10^6	10^{10}	10^5	1.67×10^1	1.11
10^7	10^{10}	10^5	1.27×10^4	1.01
10^8	10^{10}	10^5	4.20×10^6	1.00
10^4	10^{11}	10^5	1.27×10^{-2}	3.63
10^5	10^{11}	10^5	4.35	1.26
10^6	10^{11}	10^5	3.20×10^3	1.03
10^7	10^{11}	10^5	1.44×10^6	1.00
10^8	10^{11}	10^5	1.76×10^8	1.00
10^4	10^7	10^6	6.76×10^{-10}	6.55
10^5	10^7	10^6	1.62×10^{-7}	1.56
10^6	10^7	10^6	1.15×10^{-4}	1.06
10^7	10^7	10^6	1.43×10^{-1}	1.01
10^8	10^7	10^6	1.87×10^2	1.01
10^4	10^8	10^6	3.30×10^{-7}	1.62×10^1
10^5	10^8	10^6	5.14×10^{-5}	2.53
10^6	10^8	10^6	2.35×10^{-2}	1.16
10^7	10^8	10^6	1.92×10^1	1.03
10^8	10^8	10^6	1.11×10^4	1.01
10^4	10^9	10^6	4.43×10^{-5}	8.25×10^1
10^5	10^9	10^6	4.90×10^{-3}	9.13
10^6	10^9	10^6	9.65×10^{-1}	1.82
10^7	10^9	10^6	5.16×10^2	1.08
10^8	10^9	10^6	2.31×10^5	1.01
10^4	10^{10}	10^6	1.70×10^{-3}	1.11×10^2
10^5	10^{10}	10^6	1.85×10^{-1}	1.20×10^1
10^6	10^{10}	10^6	3.16×10^1	2.09
10^7	10^{10}	10^6	1.39×10^4	1.10
10^8	10^{10}	10^6	4.23×10^6	1.01
10^4	10^{11}	10^6	9.55×10^{-2}	2.73×10^1
10^5	10^{11}	10^6	1.25×10^1	3.64
10^6	10^{11}	10^6	3.92×10^3	1.25
10^7	10^{11}	10^6	1.46×10^6	1.02
10^8	10^{11}	10^6	1.76×10^8	1.00
10^4	10^7	10^7	6.29×10^{-9}	6.10×10^1
10^5	10^7	10^7	7.33×10^{-7}	7.08
10^6	10^7	10^7	1.82×10^{-4}	1.69
10^7	10^7	10^7	1.62×10^{-1}	1.15
10^8	10^7	10^7	1.98×10^2	1.06
10^4	10^8	10^7	3.32×10^{-6}	1.63×10^2

10^5	10^8	10^7	3.52×10^{-4}	1.73×10^1
10^6	10^8	10^7	5.51×10^{-2}	2.73
10^7	10^8	10^7	2.36×10^1	1.26
10^8	10^8	10^7	1.18×10^4	1.07
10^4	10^9	10^7	4.46×10^{-4}	8.30×10^2
10^5	10^9	10^7	4.50×10^{-2}	8.39×10^1
10^6	10^9	10^7	4.94	9.31
10^7	10^9	10^7	8.82×10^2	1.85
10^8	10^9	10^7	2.50×10^5	1.09
10^4	10^{10}	10^7	1.67×10^{-2}	1.09×10^3
10^5	10^{10}	10^7	1.68	1.09×10^2
10^6	10^{10}	10^7	1.77×10^2	1.17×10^1
10^7	10^{10}	10^7	2.52×10^4	2.00
10^8	10^{10}	10^7	4.53×10^6	1.08
10^4	10^{11}	10^7	9.22×10^{-1}	2.63×10^2
10^5	10^{11}	10^7	9.40×10^1	2.73×10^1
10^6	10^{11}	10^7	1.10×10^4	3.52
10^7	10^{11}	10^7	1.73×10^6	1.20
10^8	10^{11}	10^7	1.79×10^8	1.02
10^4	10^7	10^8	1.05×10^{-7}	1.01×10^3
10^5	10^7	10^8	1.06×10^{-5}	1.03×10^2
10^6	10^7	10^8	1.30×10^{-3}	1.21×10^1
10^7	10^7	10^8	3.87×10^{-1}	2.75
10^8	10^7	10^8	3.03×10^2	1.63
10^4	10^8	10^8	5.16×10^{-5}	2.53×10^3
10^5	10^8	10^8	5.20×10^{-3}	2.56×10^2
10^6	10^8	10^8	5.50×10^{-1}	2.72×10^1
10^7	10^8	10^8	8.20×10^1	4.37
10^8	10^8	10^8	1.88×10^4	1.70
10^4	10^9	10^8	5.00×10^{-3}	9.31×10^3
10^5	10^9	10^8	5.01E-01	9.34×10^2
10^6	10^9	10^8	5.00×10^1	9.43×10^1
10^7	10^9	10^8	4.91×10^3	1.03×10^1
10^8	10^9	10^8	4.42×10^5	1.93
10^4	10^{10}	10^8	1.67×10^{-1}	1.09×10^4
10^5	10^{10}	10^8	1.67×10^1	1.08×10^3
10^6	10^{10}	10^8	1.62×10^3	1.07×10^2
10^7	10^{10}	10^8	1.30×10^5	1.03×10^1
10^8	10^{10}	10^8	7.35×10^6	1.75
10^4	10^{11}	10^8	1.10×10^1	3.15×10^3
10^5	10^{11}	10^8	1.07×10^3	3.11×10^2
10^6	10^{11}	10^8	8.57×10^4	2.74×10^1
10^7	10^{11}	10^8	4.18×10^6	2.92
10^8	10^{11}	10^8	2.06×10^8	1.17

Table S16. Absolute cluster formation rate and enhancement strength of SFA (r_{SFA}) under the conditions of $[\text{SA}] = 10^4 - 10^8$ molecules cm^{-3} , $[\text{DMA}] = 10^7 - 10^{11}$ molecules cm^{-3} , $[\text{SFA}] = 10^4 - 10^8$ molecules cm^{-3} at 258K. SA, DMA and SFA are shorthand for sulfuric acid, dimethylamine and sulfamic acid, respectively.

[SA] (molecules cm^{-3})	[DMA] (molecules cm^{-3})	[SFA] (molecules cm^{-3})	Absolute cluster formation rate	Enhancement strength (r_{SFA})
10^4	10^7	10^4	5.60×10^{-9}	1.87
10^5	10^7	10^4	3.26×10^{-6}	1.09
10^6	10^7	10^4	3.10×10^{-3}	1.00
10^7	10^7	10^4	3.90	1.00
10^8	10^7	10^4	4.13×10^3	1.00
10^4	10^8	10^4	1.23×10^{-6}	2.25
10^5	10^8	10^4	6.17×10^{-4}	1.12
10^6	10^8	10^4	5.49×10^{-1}	1.01
10^7	10^8	10^4	4.86×10^2	1.00
10^8	10^8	10^4	2.15×10^5	1.00
10^4	10^9	10^4	6.88×10^{-5}	1.93
10^5	10^9	10^4	3.88×10^{-2}	1.09
10^6	10^9	10^4	3.48×10^1	1.01
10^7	10^9	10^4	2.60×10^4	1.00
10^8	10^9	10^4	5.03×10^6	1.00
10^4	10^{10}	10^4	1.44×10^{-2}	1.18
10^5	10^{10}	10^4	1.22×10^1	1.02
10^6	10^{10}	10^4	9.79×10^3	1.00
10^7	10^{10}	10^4	2.42×10^6	1.00
10^8	10^{10}	10^4	9.51×10^7	1.00
10^4	10^{11}	10^4	1.05×10^1	1.02
10^5	10^{11}	10^4	8.47×10^3	1.00
10^6	10^{11}	10^4	2.15×10^6	1.00
10^7	10^{11}	10^4	8.21×10^7	1.00
10^8	10^{11}	10^4	1.28×10^9	1.00
10^4	10^7	10^5	2.91×10^{-8}	9.73
10^5	10^7	10^5	5.61×10^{-6}	1.87
10^6	10^7	10^5	3.40×10^{-3}	1.10
10^7	10^7	10^5	3.93	1.01
10^8	10^7	10^5	4.13×10^3	1.00
10^4	10^8	10^5	7.39×10^{-6}	1.35×10^1
10^5	10^8	10^5	1.20×10^{-3}	2.19
10^6	10^8	10^5	6.09×10^{-1}	1.12
10^7	10^8	10^5	4.91×10^2	1.01
10^8	10^8	10^5	2.15×10^5	1.00
10^4	10^9	10^5	3.68×10^{-4}	1.03×10^1
10^5	10^9	10^5	6.86×10^{-2}	1.93

10^6	10^9	10^5	$3.77*10^1$	1.09
10^7	10^9	10^5	$2.61*10^4$	1.01
10^8	10^9	10^5	$5.04*10^6$	1.00
10^4	10^{10}	10^5	$3.35*10^{-2}$	2.75
10^5	10^{10}	10^5	$1.41*10^1$	1.17
10^6	10^{10}	10^5	$9.93*10^3$	1.02
10^7	10^{10}	10^5	$2.42*10^6$	1.00
10^8	10^{10}	10^5	$9.51*10^7$	1.00
10^4	10^{11}	10^5	$1.25*10^1$	1.22
10^5	10^{11}	10^5	$8.63*10^3$	1.02
10^6	10^{11}	10^5	$2.15*10^6$	1.00
10^7	10^{11}	10^5	$8.21*10^7$	1.00
10^8	10^{11}	10^5	$1.28*10^9$	1.00
10^4	10^7	10^6	$2.65*10^{-7}$	$8.85*10^1$
10^5	10^7	10^6	$2.92*10^{-5}$	9.71
10^6	10^7	10^6	$5.70*10^{-3}$	1.84
10^7	10^7	10^6	4.16	1.07
10^8	10^7	10^6	$4.16*10^3$	1.01
10^4	10^8	10^6	$6.89*10^{-5}$	$1.26*10^2$
10^5	10^8	10^6	$7.40*10^{-3}$	$1.35*10^1$
10^6	10^8	10^6	1.21	2.24
10^7	10^8	10^6	$5.42*10^2$	1.12
10^8	10^8	10^6	$2.16*10^5$	1.01
10^4	10^9	10^6	$3.30*10^{-3}$	$9.27*10^1$
10^5	10^9	10^6	$3.65*10^{-1}$	$1.03*10^1$
10^6	10^9	10^6	$6.62*10^1$	1.92
10^7	10^9	10^6	$2.81*10^4$	1.08
10^8	10^9	10^6	$5.06*10^6$	1.01
10^4	10^{10}	10^6	$2.25*10^{-1}$	$1.84*10^1$
10^5	10^{10}	10^6	$3.27*10^1$	2.73
10^6	10^{10}	10^6	$1.14*10^4$	1.16
10^7	10^{10}	10^6	$2.45*10^6$	1.01
10^8	10^{10}	10^6	$9.52*10^7$	1.00
10^4	10^{11}	10^6	$3.28*10^1$	3.18
10^5	10^{11}	10^6	$1.02*10^4$	1.21
10^6	10^{11}	10^6	$2.19*10^6$	1.02
10^7	10^{11}	10^6	$8.23*10^7$	1.00
10^8	10^{11}	10^6	$1.29*10^9$	1.00
10^4	10^7	10^7	$2.67*10^{-6}$	$8.94*10^2$
10^5	10^7	10^7	$2.70*10^{-4}$	$8.99*10^1$
10^6	10^7	10^7	$2.97*10^{-2}$	9.58
10^7	10^7	10^7	6.57	1.68
10^8	10^7	10^7	$4.43*10^3$	1.07
10^4	10^8	10^7	$6.73*10^{-4}$	$1.23*10^3$

10^5	10^8	10^7	$6.77*10^{-2}$	$1.24*10^2$
10^6	10^8	10^7	7.15	$1.32*10^1$
10^7	10^8	10^7	$1.05*10^3$	2.16
10^8	10^8	10^7	$2.33*10^5$	1.09
10^4	10^9	10^7	$3.21*10^{-2}$	$9.01*10^2$
10^5	10^9	10^7	3.23	$9.10*10^1$
10^5	10^9	10^7	$3.41*10^2$	9.89
10^7	10^9	10^7	$4.67*10^4$	1.80
10^8	10^9	10^7	$5.33*10^6$	1.06
10^4	10^{10}	10^7	2.10	$1.72*10^2$
10^5	10^{10}	10^7	$2.15*10^2$	$1.80*10^1$
10^6	10^{10}	10^7	$2.53*10^4$	2.59
10^7	10^{10}	10^7	$2.74*10^6$	1.13
10^8	10^{10}	10^7	$9.66*10^7$	1.02
10^4	10^{11}	10^7	$2.37*10^2$	$2.31*10^1$
10^5	10^{11}	10^7	$2.59*10^4$	3.06
10^6	10^{11}	10^7	$2.52*10^6$	1.17
10^7	10^{11}	10^7	$8.39*10^7$	1.02
10^8	10^{11}	10^7	$1.29*10^9$	1.00
10^4	10^7	10^8	$2.91*10^{-5}$	$9.74*10^3$
10^5	10^7	10^8	$2.90*10^{-3}$	$9.66*10^2$
10^6	10^7	10^8	$2.92*10^{-1}$	$9.40*10^1$
10^7	10^7	10^8	$3.18*10^1$	8.14
10^8	10^7	10^8	$7.03*10^3$	1.70
10^4	10^8	10^8	$6.10*10^{-3}$	$1.11*10^4$
10^5	10^8	10^8	$6.08*10^{-1}$	$1.11*10^3$
10^6	10^8	10^8	$6.02*10^1$	$1.11*10^2$
10^7	10^8	10^8	$5.52*10^3$	$1.14*10^1$
10^8	10^8	10^8	$3.77*10^5$	1.76
10^4	10^9	10^8	$2.83*10^{-1}$	$7.93*10^3$
10^5	10^9	10^8	$2.81*10^1$	$7.92*10^2$
10^6	10^9	10^8	$2.68*10^3$	$7.78*10^1$
10^7	10^9	10^8	$1.93*10^5$	7.46
10^8	10^9	10^8	$7.59*10^6$	1.51
10^4	10^{10}	10^8	$2.10*10^1$	$1.72*10^4$
10^5	10^{10}	10^8	$2.00*10^3$	$1.67*10^4$
10^6	10^{10}	10^8	$1.43*10^5$	$1.47*10^1$
10^7	10^{10}	10^8	$5.12*10^6$	2.11
10^8	10^{10}	10^8	$1.10*10^8$	1.15
10^4	10^{11}	10^8	$2.75*10^3$	$2.67*10^2$
10^5	10^{11}	10^8	$1.78*10^5$	$2.11*10^1$
10^6	10^{11}	10^8	$5.34*10^6$	2.48
10^7	10^{11}	10^8	$9.92*10^7$	1.21
10^8	10^{11}	10^8	$1.35*10^9$	1.05

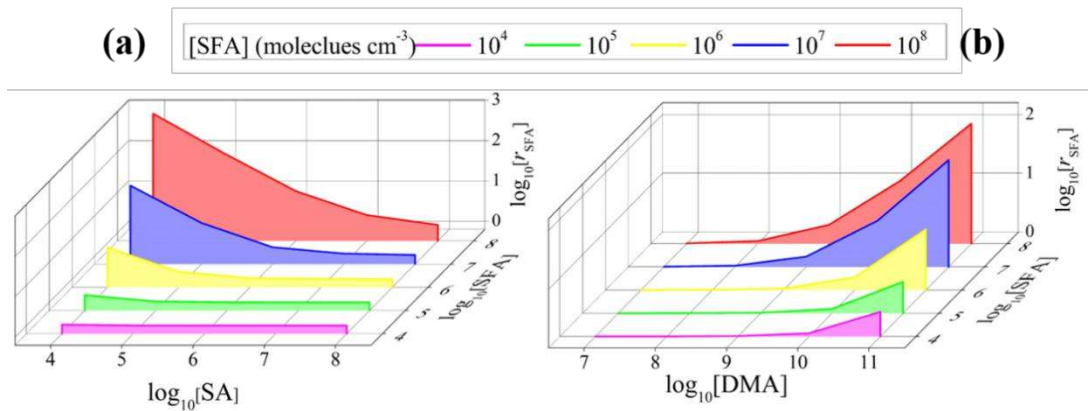


Figure S1. (a) The ratio of cluster formation rates (r_{SFA}) versus the logarithm of [SA]; at $[\text{DMA}] = 10^9$ molecules cm^{-3} , and (b) the ratio of cluster formation rates (r_{SFA}) versus the logarithm of [DMA], at $T = 298$ K and $[\text{SFA}] = 10^4\text{-}10^8$ molecules cm^{-3} . SFA, SA and DMA refer to sulfmaic acid, sulfuric acid and dimethylamine, respectively.

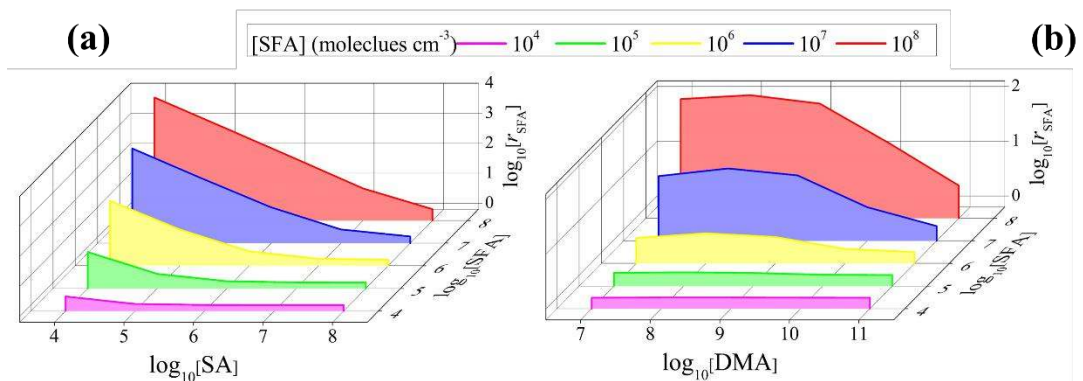


Figure S2. (a) The ratio of cluster formation rates (r_{SFA}) versus the logarithm of [SA] at $[\text{DMA}] = 10^9$ molecules cm^{-3} , and (b) the ratio of cluster formation rates (r_{SFA}) versus the logarithm of [DMA], at $T = 258$ K and $[\text{SFA}] = 10^4\text{-}10^8$ molecules cm^{-3} . SFA, SA and DMA refer to sulfmaic acid, sulfuric acid and dimethylamine, respectively.

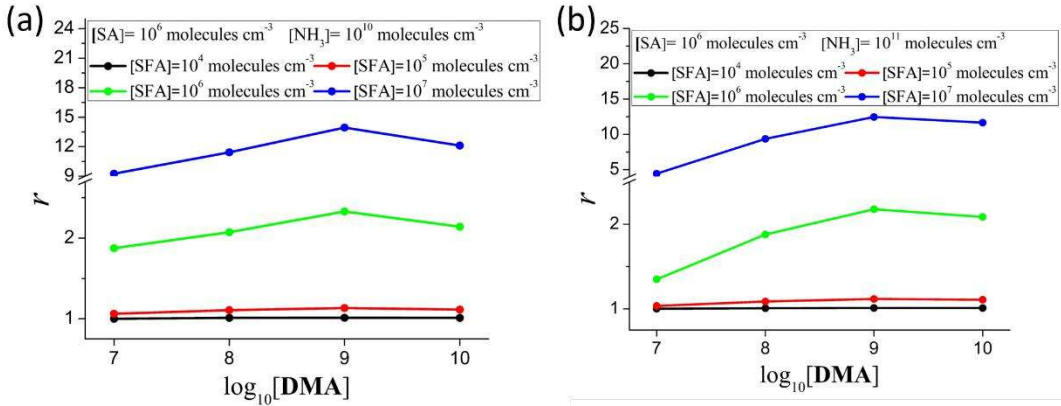


Figure S3. (a) The ratio (r) of cluster formation rates versus the logarithm of [DMA] at $[SA] = 10^6$ molecules cm^{-3} , $[\text{NH}_3] = 10^{10}$ molecules cm^{-3} , $[\text{SFA}] = 10^4\text{-}10^7$ molecules cm^{-3} and $T = 278$ K. (b) The ratio (r) of cluster formation rates versus the logarithm of [DMA] at $[SA] = 10^6$ molecules cm^{-3} , $[\text{NH}_3] = 10^{11}$ molecules cm^{-3} , $[\text{SFA}] = 10^4\text{-}10^7$ molecules cm^{-3} and $T = 278$ K. SFA, SA, DMA and NH_3 refer to sulfamic acid, sulfuric acid, dimethylamine and ammonia, respectively.

Figure S3 shows the ratio of cluster formation rates in the presence of SFA to the rates without SFA being expressed in equation S(12) at temperature $T = 278$ K.

$$r = \frac{J([\text{SFA}] = x, [\text{SA}] = 10^6, [\text{DMA}] = z, [\text{NH}_3] = 10^{10} \text{ or } 10^{11})}{J([\text{SA}] = 10^6, [\text{DMA}] = z, [\text{NH}_3] = 10^{10} \text{ or } 10^{11})} \quad \text{S(12)}$$

where $[\text{SFA}]$, $[\text{SA}]$, $[\text{DMA}]$ and $[\text{NH}_3]$ are the concentrations of SFA, SA, DMA, and NH_3 , respectively. $[\text{SA}]$ and $[\text{NH}_3]$ are set to be 10^6 and 10^{10} or 10^{11} molecules cm^{-3} , respectively. $[\text{SFA}]$ is varied from 10^4 to 10^7 molecules cm^{-3} , and $[\text{DMA}]$ ranges from 10^7 to 10^{10} molecules cm^{-3} . Here, the cluster size of the simulated systems is set to be 2×2 , containing $(\text{SFA})_x(\text{SA})_y(\text{DMA})_z(\text{NH}_3)_n$ ($x + y \leq 2$, $z + n \leq 2$) clusters. Among these clusters, only the clusters containing approximately equal numbers of acid and base molecules or the clusters with larger numbers of acid than base molecules are considered, as only these clusters have the potential to further grow into larger sizes. In addition, considering the formation Gibbs free energy (Table S1 and Table S13) and evaporation rates (Table S2 and Table S13), the clusters containing SA and DMA molecules and an SFA molecule are the most stable and therefore are allowed to form larger clusters contributing to the particle formation rates. In this case, clusters $(\text{SA})_3\cdot(\text{DMA})_2$, $(\text{SA})_3\cdot(\text{DMA})_3$, $(\text{SA})_3\cdot(\text{NH}_3)_2$, $(\text{SA})_3\cdot(\text{NH}_3)_3$, $\text{SFA}\cdot(\text{SA})_2\cdot(\text{DMA})_2$, $\text{SFA}\cdot(\text{SA})_2\cdot(\text{DMA})_3$, $\text{SFA}\cdot(\text{SA})_2\cdot(\text{NH}_3)_2$ and $\text{SFA}\cdot(\text{SA})_2\cdot(\text{NH}_3)_3$ are set as the boundary clusters. Moreover, the constant coagulation sink coefficient is also set to be $5 \times 10^{-2} \text{ s}^{-1}$ in the case of polluted areas.

Cartesian coordinates of all stable clusters involving in the system at M06-2X/6-311++G(3df,3pd) level of theory. All coordinates in Å.

Species

SA	X	Y	Z
S	0.000005	0.000016	-0.153840
O	-0.641014	1.068315	-0.819634
O	0.641010	-1.068198	-0.819791
O	1.029509	0.662883	0.836104
H	1.691757	0.010575	1.099988
O	-1.029512	-0.663010	0.836010
H	-1.691786	-0.010751	1.099948
DMA	X	Y	Z
N	0.000000	0.568582	-0.149061
H	-0.000002	1.334902	0.510561
C	1.204297	-0.224055	0.020256
H	1.261428	-0.962157	-0.780509
H	2.082747	0.414271	-0.050609
H	1.240320	-0.765268	0.976018
C	-1.204297	-0.224056	0.020255
H	-2.082746	0.414274	-0.050588
H	-1.261437	-0.962145	-0.780520
H	-1.240311	-0.765282	0.976011
SFA	X	Y	Z
S	-0.032881	0.102059	0.115903
O	0.145677	1.500741	0.002505
O	-0.619949	-0.512974	1.255086

N	1.416583	-0.578005	-0.135921
H	1.925930	-0.159242	-0.902282
H	1.398053	-1.588331	-0.156131
O	-0.902920	-0.366689	-1.136894
H	-1.696434	-0.807959	-0.810161

SA·DMA	X	Y	Z
N	1.890216	-0.112025	0.150141
H	1.501783	-0.288625	1.080366
C	2.054698	1.345910	-0.016930
H	2.344097	1.545303	-1.045177
H	1.097984	1.815042	0.196587
H	2.819059	1.713465	0.663362
C	3.100700	-0.900948	-0.119798
H	2.879903	-1.953688	0.026989
H	3.402496	-0.734534	-1.150324
H	3.902085	-0.593185	0.547723
S	-1.267258	-0.174467	0.049460
O	-2.472925	-0.936015	0.078274
O	-0.553397	0.014382	1.293566
O	-0.334197	-0.586758	-1.020314
H	1.040172	-0.404079	-0.471705
O	-1.690040	1.325006	-0.346635
H	-2.470887	1.273267	-0.908926

SFA·DMA	X	Y	Z
S	1.187822	-0.175803	-0.027610

O	2.416728	-0.904465	0.041606
O	0.383248	-0.363837	-1.216499
O	0.368651	-0.330911	1.203422
H	-0.980529	-0.140892	0.874601
N	-2.042157	0.033746	0.536094
H	-2.617014	0.114306	1.370144
C	-2.478651	-1.125403	-0.270995
H	-1.773979	-1.228067	-1.090751
H	-3.488012	-0.960918	-0.642332
H	-2.446714	-2.016991	0.348387
C	-2.064963	1.308435	-0.214746
H	-1.419608	1.184918	-1.079203
H	-1.661469	2.093441	0.418042
H	-3.083272	1.543328	-0.517318
N	1.507097	1.473171	-0.025992
H	2.117700	1.679193	0.758358
H	2.005842	1.691623	-0.882652
(SA) ₂	X	Y	Z
S	-2.035487	-0.073173	0.114174
O	-1.067162	0.084496	1.156741
O	-3.311025	-0.603152	0.396130
O	-2.180636	1.369567	-0.491854
H	-2.959535	1.415304	-1.063055
O	-1.423669	-0.890222	-1.038406
H	-0.462450	-0.657408	-1.157871

O	1.067112	-0.085041	-1.156651
S	2.035447	0.073169	-0.114181
O	1.423398	0.890156	1.038314
O	3.310760	0.603600	-0.396317
O	2.181234	-1.369418	0.492059
H	0.462241	0.657071	1.157837
H	2.960289	-1.414778	1.063076
(SFA)₂·DMA		X	Y
S	1.793468	0.035675	-0.047827
O	1.411071	1.411646	-0.089084
O	1.212038	-0.851155	-1.020098
O	1.534370	-0.553186	1.358845
S	-1.956770	-0.058064	0.084502
O	-1.514273	-0.786707	-1.227355
H	-0.537277	-0.895016	-1.249454
O	-1.083999	-0.500363	1.139538
O	-3.353887	-0.235089	0.182911
H	0.549258	-0.632959	1.464750
N	-1.653158	1.519004	-0.108418
H	-0.662439	1.743174	-0.155678
H	-2.212654	1.940916	-0.837402
N	3.403198	-0.041514	-0.117390
H	3.759713	-0.856334	-0.596016
H	3.823383	0.834835	-0.390407
SA·DMA		X	Y
		Z	

S	-1.744500	0.000006	-0.045110
O	-1.223406	-1.229294	-0.569083
O	-1.223443	1.229380	-0.568942
O	-1.584696	-0.000082	1.495231
S	1.921382	0.000002	0.080960
O	1.545041	1.225367	-0.799385
H	0.578783	1.390000	-0.771920
O	1.059267	0.000039	1.231416
O	3.317254	0.000007	0.239714
O	1.545048	-1.225413	-0.799311
H	0.578774	-1.389979	-0.771915
H	-0.613464	-0.000060	1.681734
N	-3.343405	-0.000017	-0.200489
H	-3.725461	0.856816	-0.572521
H	-3.725422	-0.856806	-0.572663
(SA)₂·DMA	X	Y	Z
S	1.417909	-1.243203	-0.105166
O	2.265192	-0.341928	-0.846672
O	0.878931	-0.613986	1.104197
O	2.412458	-2.373951	0.373709
O	0.388818	-1.915572	-0.871812
H	1.768614	1.271999	-0.418624
H	1.909171	-3.143245	0.668102
S	-2.231442	0.027253	0.027463
O	-1.695991	-0.563310	1.352618

O	-3.593987	0.346987	0.188256
O	-2.126427	-1.139575	-0.979495
O	-1.319333	1.067843	-0.390520
H	-0.692955	-0.629517	1.327177
H	-1.185009	-1.459817	-1.042313
N	1.179250	2.053474	-0.069444
H	0.240099	1.620408	0.024910
C	1.082714	3.124656	-1.081351
H	2.067091	3.554262	-1.244826
H	0.396884	3.886248	-0.721188
H	0.700213	2.695194	-2.001879
C	1.670933	2.499382	1.250010
H	2.660141	2.933013	1.131871
H	1.712728	1.633768	1.903168
H	0.985638	3.242274	1.648754

SFA·SA·DMA	X	Y	Z
S	-1.571913	-1.102312	-0.100132
O	-0.900868	-0.591316	1.111663
O	-0.613347	-1.623781	-1.054606
O	-2.494132	-0.109487	-0.615258
S	2.240516	-0.160895	0.020604
O	1.970052	-1.226254	-1.063836
H	0.988922	-1.400034	-1.144208
O	1.474943	1.021775	-0.307850
O	3.635410	-0.031694	0.175249

O	1.646657	-0.767448	1.309436
H	0.634925	-0.740780	1.284419
H	-1.704698	1.424988	-0.327965
N	-2.511493	-2.391495	0.283303
H	-1.949461	-3.167406	0.611365
H	-3.223103	-2.137404	0.957053
N	-0.971730	2.116800	-0.074459
H	-0.081374	1.574414	-0.084790
C	-1.205795	2.610534	1.297845
H	-2.129975	3.181574	1.319610
H	-1.274997	1.749683	1.955188
H	-0.370578	3.241354	1.589782
C	-0.867607	3.179363	-1.093542
H	-0.706725	2.716782	-2.062244
H	-1.785041	3.761257	-1.103871
H	-0.022262	3.816020	-0.848004
(SFA)₂·DMA			
	X	Y	Z
S	1.564233	-1.150931	-0.116786
O	0.608229	-1.827766	-0.953826
O	0.926196	-0.569612	1.086837
O	2.390271	-0.141290	-0.761988
S	-2.280182	-0.087648	0.056185
O	-1.608162	-0.718343	1.301037
H	-0.593357	-0.709542	1.224658
O	-1.443128	1.003405	-0.385996

O	-3.635224	0.162206	0.385466
H	1.665535	1.338627	-0.403801
N	-2.242682	-1.184189	-1.136129
H	-1.288458	-1.498047	-1.320301
H	-2.874641	-1.950897	-0.942777
N	2.630591	-2.315850	0.345693
H	3.331610	-1.940454	0.972225
H	2.144011	-3.097735	0.766815
N	1.016417	2.094300	-0.082816
H	0.100061	1.612048	-0.003247
C	0.889751	3.147776	-1.107516
H	1.856240	3.620960	-1.258026
H	0.547014	2.691473	-2.030864
H	0.162480	3.881863	-0.771464
C	1.447194	2.579642	1.242423
H	1.504556	1.724585	1.908241
H	2.421362	3.052020	1.147543
H	0.721351	3.299244	1.611709
(SA)₃	X	Y	Z
S	0.167920	1.320040	-0.057413
O	-0.089832	0.122803	-0.837861
O	1.368633	2.008916	-0.384246
H	3.071995	1.295410	-0.300466
O	0.134874	0.940175	1.435606
O	-1.003413	2.277486	-0.162654

O	3.782072	0.624133	-0.246015
S	3.189528	-0.772190	0.086628
O	4.262284	-1.665784	0.230753
O	2.405788	-1.159184	-1.203414
O	-2.385128	-1.251101	-1.033293
H	1.501630	-0.787064	-1.195035
H	-1.502717	-0.804808	-1.022446
O	2.229806	-0.619041	1.147858
O	-3.143597	0.853129	-0.090102
H	0.887422	0.312074	1.592678
H	-1.882581	1.788015	-0.119937
O	-4.637308	-1.102728	-0.248839
S	-3.352712	-0.563822	-0.047139
O	-2.803848	-0.987933	1.360049
H	-3.114193	-1.875048	1.589263
(SFA) ₃	X	Y	Z
S	1.260030	1.977987	-0.068165
O	1.171923	3.381846	-0.192254
O	0.271621	1.116617	-0.667726
N	1.254431	1.604464	1.512372
H	1.911231	2.162104	2.043392
H	1.324333	0.604428	1.684073
O	2.641253	1.553926	-0.644652
H	2.686766	0.570289	-0.703889
S	1.306386	-1.799878	0.021697

O	2.478637	-1.122926	-0.451331
O	0.634321	-1.282167	1.178650
N	1.796651	-3.302195	0.383300
H	2.353171	-3.713636	-0.355848
H	1.033787	-3.898961	0.679368
O	0.311756	-1.933248	-1.134222
H	-0.619117	-1.570079	-0.921381
S	-2.722266	-0.066706	-0.042047
O	-4.128862	-0.095182	0.062147
O	-2.037939	-1.185963	-0.647089
N	-2.070849	0.084569	1.428307
H	-2.373691	0.911852	1.924598
H	-1.069421	-0.083454	1.444713
O	-2.370658	1.218197	-0.845398
H	-1.391495	1.318325	-0.911656
SFA·(SA)₂	X	Y	Z
S	-0.012806	-2.364230	0.081115
O	-0.298623	-3.660427	0.605699
O	-0.262394	-1.172579	0.926531
O	1.484947	-2.331682	-0.371171
H	1.704606	-1.428364	-0.741363
O	-0.825215	-2.150192	-1.251159
H	-1.077779	-1.197669	-1.375358
S	-2.024577	1.116087	-0.043292
O	-0.916595	1.866807	0.524800

O	-1.827968	0.375199	-1.277595
N	-3.257430	2.150681	-0.289034
H	-3.479901	2.705459	0.534498
H	-4.070992	1.704918	-0.707234
O	-2.591706	0.142778	1.078258
H	-1.880793	-0.515962	1.297737
S	2.231957	1.138174	-0.069116
O	3.650964	1.298044	-0.097524
O	1.561545	0.234171	-1.011897
O	1.791441	0.681236	1.383399
H	0.992576	0.100989	1.327564
O	1.594345	2.570280	-0.221640
H	0.615167	2.506276	-0.113525
(SFA)₂·SA	X	Y	Z
S	-3.528465	-0.565844	0.093922
O	-4.689633	-1.355206	0.228883
O	-2.575760	-0.471545	1.168802
N	-3.979596	0.942718	-0.258849
H	-4.708830	0.975146	-0.959182
H	-3.194593	1.560682	-0.442506
O	-2.753067	-1.128259	-1.151841
H	-1.803802	-0.915458	-1.106955
S	3.539697	-0.599038	0.013420
O	4.702833	-1.363052	0.234948
O	2.270035	-1.258675	-0.159237

N	3.758725	0.318929	-1.303309
H	2.995724	0.968482	-1.463984
H	4.669520	0.761075	-1.312065
O	3.406902	0.372856	1.234177
H	2.614511	0.931792	1.122553
S	-0.034246	1.068730	-0.025432
O	1.276759	1.642097	-0.068108
O	-1.135537	1.778232	-0.573116
O	-0.008747	-0.303294	-0.758428
H	0.861985	-0.780284	-0.557855
O	-0.285974	0.704111	1.447280
H	-1.182677	0.267363	1.517675
(SA)₂·(DMA)₂			
	X	Y	Z
S	-1.606855	1.347518	-0.541841
O	-0.703329	2.430901	-0.902375
O	-1.341294	0.174404	-1.582676
O	-1.194162	0.778567	0.761290
O	-3.003140	1.608462	-0.643145
H	-1.354431	-0.793642	0.764883
N	1.404337	1.921073	0.714342
H	0.710844	2.136148	-0.043365
H	1.275004	0.916270	0.911732
O	0.726982	-2.463928	-0.721471
O	1.573538	-0.925165	0.967359
S	1.565542	-1.321227	-0.424960

O	1.339643	-0.199856	-1.327488
O	3.066730	-1.789303	-0.675162
H	3.129947	-2.173074	-1.558277
H	-0.370526	0.042400	-1.671423
H	-1.004629	-2.165216	-0.099426
N	-1.601030	-1.822148	0.666001
C	-3.034842	-1.890032	0.319249
C	-1.228313	-2.540144	1.899689
C	1.029122	2.713107	1.901850
C	2.787293	2.141359	0.251590
H	2.957127	1.517119	-0.619576
H	3.474722	1.867574	1.047666
H	2.912204	3.190421	-0.003018
H	1.133231	3.768751	1.666531
H	1.682895	2.450424	2.729454
H	-0.004252	2.483667	2.141149
H	-1.762133	-2.097011	2.736302
H	-1.495949	-3.589149	1.802512
H	-0.155985	-2.435168	2.037432
H	-3.328024	-2.928023	0.184850
H	-3.605827	-1.440269	1.127051
H	-3.195660	-1.322765	-0.592993
SFA·SA·(DMA)₂			
	X	Y	Z
S	-1.764807	1.186705	-0.528154
O	-3.178600	1.318118	-0.637849

O	-1.308702	0.654735	0.775877
O	-1.383454	0.049948	-1.572244
H	-0.402973	0.008994	-1.654452
O	-0.964181	2.351434	-0.879269
H	1.174186	1.018230	0.918268
S	1.699416	-1.147135	-0.436378
O	1.308846	-0.065761	-1.333051
O	1.627620	-0.777428	0.970907
N	3.319967	-1.336204	-0.734722
H	3.456965	-1.587117	-1.707769
H	3.692421	-2.065811	-0.137466
O	1.004566	-2.394566	-0.719060
H	-0.700453	-2.249979	-0.069742
N	-1.375219	-1.979453	0.663113
H	-1.268888	-0.927309	0.762900
C	-0.971984	-2.634493	1.921179
H	-1.089857	-3.710629	1.821619
H	0.067956	-2.384458	2.109733
H	-1.602747	-2.266273	2.726026
C	-2.769034	-2.241459	0.252843
H	-2.962423	-1.704777	-0.671182
H	-2.912508	-3.310165	0.115163
H	-3.433395	-1.871561	1.029261
N	1.192662	2.031260	0.718000
H	0.474114	2.171552	-0.034320

C	2.539829	2.395671	0.241187
H	3.259031	2.211973	1.035134
H	2.773218	1.779711	-0.621458
H	2.546004	3.448263	-0.029631
C	0.744414	2.783478	1.905639
H	-0.253835	2.441094	2.158733
H	1.433860	2.602333	2.726322
H	0.725594	3.842559	1.663072

	X	Y	Z
(SFA) ₂ ·(DMA) ₂			
H	-0.457581	-1.418567	0.263061
S	2.645717	0.075518	-0.173992
O	2.451930	-1.107679	-1.003248
O	2.909192	1.286319	-0.912207
O	1.564283	0.246396	0.803766
N	0.176532	-2.216869	0.033383
H	0.991786	-1.819253	-0.479918
C	-0.536735	-3.203277	-0.801804
H	-1.408434	-3.558745	-0.260360
H	0.137961	-4.025497	-1.026524
H	-0.872161	-2.717982	-1.711630
C	0.682171	-2.768192	1.306709
H	-0.160566	-3.116943	1.897835
H	1.211103	-1.975824	1.826962
H	1.357061	-3.592655	1.092090
H	0.457369	1.418592	0.262880

S	-2.645703	-0.075552	-0.174014
O	-1.564321	-0.246108	0.803858
O	-2.452040	1.107537	-1.003449
O	-2.908902	-1.286529	-0.912049
N	-0.176624	2.216937	0.033008
H	-0.991885	1.819331	-0.480278
C	0.536898	3.203060	-0.802298
H	1.408607	3.558471	-0.260833
H	-0.137621	4.025361	-1.027252
H	0.872337	2.717527	-1.711992
C	-0.682278	2.768579	1.306188
H	0.160475	3.117231	1.897350
H	-1.211441	1.976411	1.826512
H	-1.356954	3.593164	1.091366
N	3.964074	-0.322772	0.764023
H	4.731717	-0.575268	0.151152
H	4.233221	0.481163	1.320594
N	-3.964208	0.322669	0.763818
H	-4.731830	0.574972	0.150843
H	-4.233288	-0.481224	1.320481
(SA)₃·DMA			
	X	Y	Z
S	-1.108669	1.716826	-0.820797
O	-1.887694	1.490082	0.392170
O	0.307672	1.856077	-0.530479
O	-1.623186	3.130582	-1.290635

O	-1.394254	0.792458	-1.894356
H	-0.579970	0.956421	1.690216
H	-1.273141	3.334454	-2.167669
S	-1.735384	-1.842875	0.030860
O	-2.824602	-0.941109	0.658106
O	-0.457220	-1.220122	0.326328
O	-1.963397	-1.744667	-1.490261
O	-1.962642	-3.169642	0.438985
H	-2.592503	0.022694	0.542830
H	-1.744908	-0.823481	-1.797495
N	0.305922	0.809955	2.188580
H	0.962358	0.424085	1.483847
C	0.144066	-0.178171	3.276581
H	-0.539552	0.219644	4.021341
H	1.118567	-0.359122	3.721261
H	-0.246645	-1.097254	2.852623
C	0.841685	2.114501	2.635092
H	0.172652	2.539117	3.378237
H	0.912662	2.763926	1.768828
H	1.827057	1.951894	3.062252
S	2.795194	-0.537559	-0.531566
O	4.126395	-0.886387	-0.826930
O	2.335174	0.527697	-1.554773
O	2.458085	-0.061771	0.788397
H	1.545668	1.032059	-1.224874

O	1.904930	-1.769955	-0.834228
H	1.009475	-1.660322	-0.436040
SFA·(SA)₂·DMA		X	Y
S	-1.308023	1.638429	-0.803118
O	-2.032985	1.305926	0.431546
O	0.112513	1.841997	-0.569883
O	-1.592220	0.693681	-1.870223
H	-0.636333	0.922481	1.668851
S	-1.516868	-1.983532	0.037281
O	-2.649598	-1.199483	0.740741
O	-0.285649	-1.257165	0.296978
O	-1.824447	-1.863243	-1.465184
O	-1.602205	-3.335926	0.418091
H	-2.525983	-0.213070	0.608980
H	-1.718135	-0.907181	-1.749360
N	0.262898	0.843858	2.159154
H	0.939933	0.502075	1.450933
C	0.178638	-0.141795	3.257363
H	-0.515209	0.221517	4.010284
H	1.168870	-0.261806	3.687721
H	-0.164831	-1.086095	2.847683
C	0.709677	2.187676	2.585434
H	0.017885	2.575794	3.327746
H	0.730293	2.827912	1.709497
H	1.707084	2.098985	3.006306

S	2.826220	-0.322171	-0.557872
O	4.183004	-0.457248	-0.908361
O	2.116733	0.532168	-1.633162
O	2.477810	0.215620	0.735374
H	1.324475	1.011100	-1.265814
O	2.170195	-1.720715	-0.691017
H	1.244581	-1.693958	-0.352938
N	-1.873407	3.124233	-1.203617
H	-1.366768	3.490832	-2.001627
H	-2.868668	3.090982	-1.393637

(SFA) ₂ ·SA·DMA	X	Y	Z
S	-1.550948	-1.530421	-0.787098
O	-1.800159	-0.555438	-1.841869
O	-0.157958	-1.880953	-0.628864
N	-2.305966	-2.941249	-1.162878
H	-1.867415	-3.366406	-1.971727
H	-3.293185	-2.785281	-1.332421
O	-2.185217	-1.124521	0.479470
H	0.877669	-0.603218	1.348427
S	2.950252	0.171149	-0.535558
O	4.325750	0.383752	-0.783501
O	2.509780	-0.358703	0.729628
N	2.369903	-0.834363	-1.657394
H	1.413115	-1.141452	-1.484251
H	2.563001	-0.531139	-2.601950

O	2.256174	1.554814	-0.734954
H	1.333155	1.534385	-0.385371
N	0.224326	-0.940824	2.075522
H	-0.701396	-0.970134	1.628539
C	0.234298	0.017330	3.200668
H	1.250602	0.093674	3.576534
H	-0.098961	0.982838	2.834298
H	-0.429369	-0.343196	3.981611
C	0.644845	-2.309453	2.444714
H	0.608607	-2.923402	1.550724
H	1.661302	-2.262375	2.824678
H	-0.028124	-2.696784	3.204556
S	-1.368248	2.082576	0.076368
O	-1.301007	3.438679	0.449696
O	-0.200979	1.241042	0.277254
O	-2.529957	1.412110	0.845114
H	-2.506563	0.416513	0.702687
O	-1.766156	1.985963	-1.405737
H	-1.774202	1.016954	-1.684669
(SFA)₃·DMA			
	X	Y	Z
N	0.761315	-1.337597	1.913939
H	-0.003264	-1.088603	1.267420
C	0.361318	-0.943585	3.278003
H	1.154445	-1.205616	3.973109
H	0.183151	0.126116	3.284822

H	-0.551793	-1.474013	3.534227
C	1.027049	-2.781134	1.758296
H	1.298791	-2.960496	0.723159
H	1.836499	-3.069269	2.423534
H	0.119481	-3.326413	2.000683
S	-2.207489	-1.327724	-0.687866
O	-2.640665	-2.446244	-1.448540
O	-1.624103	-1.561507	0.607332
N	-3.473867	-0.342207	-0.489848
H	-4.023041	-0.281846	-1.337506
H	-3.191790	0.571990	-0.138378
O	-1.205267	-0.466756	-1.506511
H	-0.243003	-0.690411	-1.304565
S	-0.661344	2.193416	0.359668
O	-2.084593	2.182977	0.273330
O	0.027833	1.118050	1.006764
N	-0.275013	3.545693	1.194351
H	-0.741307	4.361648	0.817343
H	0.728075	3.675566	1.251642
O	-0.095199	2.368973	-1.056480
H	0.797513	1.866412	-1.173564
S	2.380692	-0.148618	-0.800724
O	2.093054	1.185531	-1.313671
O	2.921990	-0.205135	0.539344
N	3.603709	-0.663614	-1.772023

H	3.315317	-0.661751	-2.743245
H	3.923130	-1.581576	-1.488486
O	1.229745	-1.051289	-0.946337
H	1.582483	-0.799325	1.587986
(SA)₃·(DMA)₂		X	Y
S	-3.820014	-0.615076	-0.490848
O	-5.118603	-0.478446	-1.021317
O	-3.336607	0.353543	0.458466
O	-3.703133	-2.018247	0.146738
H	-2.800381	-2.120987	0.548316
O	-2.817924	-0.652183	-1.678371
H	-1.879283	-0.606434	-1.346474
N	3.743757	-1.490588	-0.159776
H	3.393621	-0.678859	0.399544
C	4.824921	-1.037919	-1.063675
H	5.135638	-1.871613	-1.687433
H	5.658054	-0.694299	-0.457397
H	4.452590	-0.216441	-1.667527
C	4.122445	-2.600481	0.740010
H	4.448533	-3.446968	0.141933
H	3.251877	-2.870556	1.328422
H	4.933347	-2.267314	1.381279
S	2.403701	1.540520	-0.321771
O	1.289317	2.457147	-0.196182
O	3.652470	2.074822	-0.746983

O	2.526412	0.707135	0.903480
H	1.133564	0.139125	1.497798
O	2.011940	0.503146	-1.462470
H	1.096153	0.171631	-1.311488
S	-0.072729	-1.289464	0.524079
O	0.237254	-0.273366	1.680162
O	-0.406511	-0.435960	-0.645792
O	1.129436	-2.048334	0.284292
H	2.901835	-1.756011	-0.679264
O	-1.207627	-2.043831	0.982854
H	-1.678499	1.180377	0.554884
N	-1.271625	2.120141	0.625199
H	-0.258767	2.062145	0.405652
C	-1.470430	2.612788	2.002200
H	-2.537014	2.644655	2.206299
H	-1.035318	3.604554	2.088241
H	-0.981960	1.924970	2.685262
C	-1.909582	2.959331	-0.410742
H	-2.976908	3.001556	-0.216049
H	-1.728155	2.502337	-1.379179
H	-1.464700	3.949872	-0.379910
SFA·(SA)₂·(DMA)₂		X	Y Z
S	3.864395	-0.449805	0.123514
O	5.247183	-0.161903	0.228384
O	2.953069	0.536073	-0.382186

O	3.737025	-1.728878	-0.745443
H	2.771898	-1.970215	-0.841715
N	0.883247	2.296651	-0.119025
H	1.026659	1.318882	-0.405265
C	1.216091	2.435132	1.316226
H	1.159247	3.486760	1.583934
H	2.216972	2.045678	1.475919
H	0.487934	1.872715	1.892499
C	1.701934	3.161071	-0.997428
H	1.478469	4.199054	-0.767447
H	1.449568	2.943815	-2.030592
H	2.748518	2.937859	-0.819256
S	0.083826	-1.407592	-0.470732
O	-1.201249	-2.075800	-0.410823
O	1.201922	-2.296399	-0.666998
O	0.066273	-0.259014	-1.376103
H	-1.452177	0.373204	-1.474711
O	0.338613	-0.792148	0.969321
H	-0.424451	-0.172654	1.135938
S	-2.472139	1.524697	0.018842
O	-2.380205	0.701732	-1.327762
O	-1.747271	0.724233	1.019612
O	-1.828287	2.801605	-0.206889
H	-0.126948	2.518020	-0.243021
O	-3.886874	1.557547	0.284057

H	-4.047873	-0.343970	0.233758
N	-3.735225	-1.327712	0.258850
H	-2.737026	-1.335337	-0.033096
C	-4.488116	-2.139303	-0.717940
H	-5.536163	-2.167994	-0.433125
H	-4.069894	-3.141833	-0.726430
H	-4.375078	-1.684288	-1.697120
C	-3.792337	-1.826729	1.648095
H	-4.827186	-1.858779	1.977406
H	-3.216791	-1.146141	2.268188
H	-3.353764	-2.820291	1.674654
N	3.309574	-0.824048	1.611192
H	2.314686	-1.035928	1.601595
H	3.865877	-1.547020	2.049693
(SFA)₂·SA·(DMA)₂		X	Y
N	-0.541635	2.315336	0.013809
H	-0.885035	1.358757	-0.134807
C	-0.701744	3.074098	-1.243923
H	-0.325952	4.082170	-1.092208
H	-0.119461	2.578609	-2.015072
H	-1.754311	3.084072	-1.508301
C	-1.262016	2.900667	1.164959
H	-2.315579	2.959311	0.910909
H	-1.118857	2.251090	2.023005
H	-0.855387	3.888792	1.363102

N	1.972577	-2.263817	-0.605897
H	1.588223	-2.183745	0.357489
C	3.387579	-2.685600	-0.567345
H	3.769861	-2.720984	-1.583769
H	3.941632	-1.955396	0.013821
H	3.452614	-3.668482	-0.108525
C	1.095620	-3.161982	-1.383158
H	0.082206	-2.777252	-1.337289
H	1.440708	-3.191905	-2.412993
H	1.135147	-4.156421	-0.947461
S	2.912233	0.994846	-0.345645
O	2.208408	2.250618	-0.126801
O	2.865201	0.131709	0.836107
N	4.526994	1.296203	-0.544193
H	4.885685	1.803379	0.257064
H	4.672317	1.833552	-1.391266
O	2.518399	0.315823	-1.565789
H	1.937220	-1.305846	-0.997336
S	-3.580360	-0.216209	-0.738483
O	-4.650113	-0.369197	-1.655293
O	-2.493819	-1.267235	-1.127429
N	-4.122570	-0.613229	0.738086
H	-3.359928	-0.648364	1.415763
H	-4.661083	-1.469769	0.712227
O	-2.912186	1.047906	-0.597399

H	0.472593	2.230336	0.204650
S	-0.234173	-0.819282	1.487974
O	-1.524503	-0.728218	2.109044
O	0.527673	-2.023701	1.748453
O	-0.292089	-0.567435	0.024614
H	-1.623201	-1.027699	-0.683680
O	0.578049	0.390043	2.071161
H	1.513052	0.339042	1.723978
(SFA)₂·(DMA)₂			
	X	Y	Z
N	3.695277	-1.214953	0.150770
H	4.042132	-0.250822	0.042168
C	4.368890	-2.130602	-0.789297
H	3.894067	-3.104623	-0.711730
H	4.240826	-1.738210	-1.793235
H	5.423836	-2.199474	-0.538676
C	3.767051	-1.630442	1.566295
H	3.272939	-0.868672	2.160809
H	3.244385	-2.577642	1.666989
H	4.807601	-1.732127	1.862226
N	-0.824593	2.175736	0.343186
H	-0.839905	1.164658	0.143185
C	-1.935190	2.837061	-0.376502
H	-1.820781	3.912582	-0.272022
H	-1.893922	2.384552	-1.423822
H	-2.879015	2.512432	0.052076

C	-0.862643	2.392169	1.805324
H	0.023712	1.937242	2.236706
H	-0.854073	3.461992	1.996112
H	-1.768964	1.940104	2.196792
S	-3.702780	-0.280205	-0.087278
O	-2.794098	0.083222	0.970430
O	-4.929654	0.419008	-0.229991
N	-4.027545	-1.854979	0.106083
H	-4.710636	-2.174587	-0.569114
H	-3.166365	-2.404079	0.091723
O	-2.931421	-0.121146	-1.428199
H	-1.944678	-0.334635	-1.288844
S	2.408802	1.604725	-0.282200
O	3.843714	1.726596	-0.160872
O	1.801511	0.813149	0.785323
N	2.201911	0.642582	-1.626674
H	2.463624	1.151204	-2.462858
H	1.241684	0.302972	-1.677873
O	1.701794	2.865759	-0.481687
H	0.095987	2.516214	-0.019532
S	-0.154126	-1.646631	-0.042473
O	-0.472159	-0.451300	-0.886950
O	-1.203626	-2.626213	-0.140841
N	-0.122929	-1.181868	1.534329
H	-1.058054	-0.909402	1.824394

H	0.542944	-0.420508	1.641685
O	1.188736	-2.104600	-0.332852
H	2.690454	-1.195959	-0.109619
(SA)₃·(DMA)₃		X	Y
S	-0.606293	-1.894692	-0.734195
O	0.570179	-2.736516	-0.724251
O	-1.758994	-2.532896	-1.344580
O	-0.941045	-1.321828	0.566756
O	-0.210595	-0.680439	-1.660339
H	0.354519	2.399278	-0.277117
N	2.672519	-2.399600	0.922299
H	1.927661	-2.342989	0.194029
H	3.349805	-1.631066	0.719728
O	1.704984	0.438868	0.366564
O	4.056998	-0.157454	0.207228
S	2.917228	0.465045	-0.439425
O	3.202667	1.780530	-0.982703
O	2.619720	-0.501569	-1.662664
H	1.655731	-0.549255	-1.810825
H	-3.132311	-1.841980	-0.665973
H	1.911518	2.802110	-0.552075
N	1.017911	3.176441	-0.165714
C	1.198824	3.458875	1.276121
C	0.524333	4.330236	-0.943701
C	3.315971	-3.719914	0.804446

C	2.023014	-2.156335	2.226726
H	1.598347	-1.157643	2.201995
H	2.764675	-2.241726	3.016741
H	1.235742	-2.893007	2.364161
H	2.388214	-4.489534	0.924713
H	4.078021	-3.821157	1.572586
H	3.766673	-3.801795	-0.179763
H	-0.441889	4.621617	-0.542350
H	1.241736	5.141961	-0.860006
H	0.419321	4.030696	-1.981854
H	1.948036	4.239232	1.381390
H	0.243712	3.773477	1.685578
H	1.528208	2.541559	1.752371
S	-1.946826	1.812183	0.463522
O	-1.958693	3.212121	0.760799
O	-1.302750	1.511086	-0.830119
O	-3.231458	1.143026	0.587168
H	-0.658278	0.161569	-1.338819
O	-0.979392	1.188610	1.542343
H	-0.763500	0.267637	1.268627
N	-3.860257	-1.338414	-0.110928
C	-4.035885	-2.024918	1.183587
C	-5.106342	-1.185079	-0.881424
H	-3.477920	-0.380964	0.094143
H	-4.460135	-3.011350	1.014374

H	-3.059322	-2.109070	1.649789
H	-4.699515	-1.431706	1.807428
H	-5.534066	-2.164649	-1.078873
H	-5.803572	-0.582833	-0.304874
H	-4.880833	-0.683474	-1.817309
SFA·(SA)₂·(DMA)₃		X	Y
N	-0.262223	0.545689	2.237321
H	-1.038229	0.594356	1.531324
C	-0.399713	1.721417	3.118939
H	0.374901	1.690267	3.880919
H	-0.288390	2.613078	2.510150
H	-1.385123	1.695506	3.576103
C	-0.362991	-0.746365	2.942726
H	-0.228720	-1.546991	2.220082
H	0.398899	-0.791473	3.717725
H	-1.354459	-0.827046	3.380250
N	3.379567	-1.316803	0.149349
H	2.713751	-1.693245	-0.552071
C	3.545430	-2.349674	1.190570
H	4.129188	-1.938397	2.009590
H	2.560341	-2.649157	1.537380
H	4.052676	-3.210311	0.763309
C	4.642868	-0.878563	-0.479243
H	4.412531	-0.100884	-1.200880
H	5.295192	-0.478859	0.292427

H	5.115178	-1.727350	-0.966259
N	-1.293609	1.641635	-1.599952
H	-0.585630	1.697733	-0.851626
C	-2.148361	2.843391	-1.503903
H	-2.922807	2.782826	-2.263685
H	-2.596199	2.858675	-0.515764
H	-1.530564	3.723688	-1.660839
C	-0.612956	1.501086	-2.902980
H	-0.129460	0.529446	-2.940373
H	-1.356117	1.570378	-3.693236
H	0.124254	2.292893	-3.004833
S	-3.325688	-0.265400	0.339774
O	-4.720894	-0.115911	0.567411
O	-2.511265	0.837937	0.874883
O	-2.886928	-1.552117	1.139998
H	-2.101894	-1.988416	0.734496
O	-2.936003	-0.511986	-1.057603
H	-1.867528	0.793098	-1.405941
S	2.100252	1.906929	0.050210
O	3.140330	2.851237	-0.165143
O	2.358975	0.959508	1.162451
O	0.746159	2.432032	0.162642
H	0.635218	0.608256	1.737498
O	2.096348	0.980416	-1.244902
H	1.366082	0.319068	-1.111946

S	0.061262	-2.010472	-0.843265
O	-0.662524	-2.752523	0.175645
O	0.169529	-0.591883	-0.468027
N	-0.783949	-2.001089	-2.253557
H	-1.740436	-1.698557	-2.056812
H	-0.766589	-2.925854	-2.667865
O	1.350211	-2.593752	-1.178036
H	2.925048	-0.467073	0.570027

Supporting References:

1. Ortega, I. K.; Kupiainen, O.; Kurtén, T.; Olenius, T.; Wilkman, O.; McGrath, M. J.; Loukonen, V.; Vehkamäki, H. *Atmos. Chem. Phys.* **2012**, *12*, 225.
2. Bork, N.; Elm, J.; Olenius, T.; Vehkamäki, H. *Atmos. Chem. Phys.* **2014**, *14*, 12023.
3. Bork, N.; Du, L.; Kjaergaard, H. G. *J. Phys. Chem. A.* **2014**, *118*, 5316.
4. Bork, N.; Du, L.; Kjaergaard, H. G. *J. Phys. Chem. A.* **2014**, *118*, 1384.
5. Ma, Y.; Chen, J.; Jiang, S.; Liu, YR.; Huang, T.; Miao, SK.; Wang, CY.; Huang, W. *RSC Adv.* **2016**, *6*, 5824.
6. Myllys, N.; Elm, J.; Halonen, R.; Kurtén, T.; Vehkamäki, H. *J. Phys. Chem. A.* **2016**, *120*, 621.
7. Nadykto, A. B.; Herb, J.; Yu, F.; Nazarenko, E. S.; Xu, Y. *CHEM PHYS LETT.* **2015**, *624*, 111.
8. Nadykto, A. B.; Nazarenko, K. M.; Yu, F. *AIP Conference Proceedings.* **2016**, *1738*, 090010.

9. Zhao, Y.; Truhlar, D. G. *Theor. Chem. Acc.* **2008**, *120*, 215.
10. Elm, J.; Bilde, M.; Mikkelsen, K. V. *J. Phys. Chem. A.* **2013**, *117*, 6695.
11. Elm, J.; Bilde, M.; Mikkelsen, K. V. *J. Chem. Theory Comput.* **2012**, *8*, 2071.
12. Long, B.; Bao, J. L.; Truhlar, G. *Phys. Chem. Chem. Phys.*, **2017**, *19*, 8091.
13. Seinfeld, J. H.; and S. N. Pandis. **2006**, 2nd ed., John Wiley, New York.
14. Holland, F.; Hofzumahaus, A.; Schäfer, J.; Kraus, A.; & Pätz, H. W. *J. Geophys. Res. Atmos.* **2003**, *9*, 1665.
15. Bandyopadhyay, B.; Kumar, P.; Biswas, P. *J. Phys. Chem. A* **2017**, *121*, 3101.
16. Battye, W. H.; Bray, C. D.; Aneja, V. P.; Tong, D.; Lee, P.; Tang, Y. *Atmos. Environ.* **2017**, *163*, 65.